

<https://helda.helsinki.fi>

Identifying dominant environmental predictors of freshwater wetland methane fluxes across diurnal to seasonal time scales

Knox, Sara H.

2021-08

Knox, S H, Bansal, S, McNicol, G, Schafer, K, Sturtevant, C, Ueyama, M, Valach, A, C, Baldocchi, D, Delwiche, K, Desai, A R, Euskirchen, E, Liu, J, Lohila, A, Malhotra, A, Melling, L, Riley, W, Runkle, B R K, Turner, J, Vargas, R, Zhu, Q, Aalto, T, Fluet-Chouinard, E, Goeckede, M, Melton, J R, Sonntag, O, Vesala, T, Ward, E, Zhang, Z, Feron, S, Ouyang, Z, Alekseychik, P, Aurela, M, Bohrer, G, Campbell, D I, Chen, J, Chu, H, Dalmagro, H J, Goodrich, J P, Gottschalk, P, Hirano, T, Iwata, H, Jurasinski, G, Kang, M, Koebsch, F, Mammarella, I, Nilsson, M B, Ono, K, Peichl, M, Peltola, O, Ryu, Y, Sachs, T, Sakabe, A, Sparks, J P, Tuittila, E-S, Vourlitis, G L, Wong, G X, Windham-Myers, L, Poulter, B & Jackson, R B 2021, ' Identifying dominant environmental predictors of freshwater wetland methane fluxes across diurnal to seasonal time scales ', *Global Change Biology*, vol. 27, no. 15, pp. 3582-3604 . <https://doi.org/10.1111/gcb.15661>

<http://hdl.handle.net/10138/346538>

<https://doi.org/10.1111/gcb.15661>

acceptedVersion

Downloaded from Helda, University of Helsinki institutional repository.

This is an electronic reprint of the original article.

This reprint may differ from the original in pagination and typographic detail.

Please cite the original version.

1 **Identifying dominant environmental predictors of freshwater wetland methane fluxes**
 2 **across diurnal to seasonal time scales**

3
 4 Running title: Dominant predictors of wetland methane fluxes

5
 6 Sara Helen Knox¹, Sheel Bansal², Gavin McNicol³, Karina Schafer⁴, Cove Sturtevant⁵, Masahito
 7 Ueyama⁶, Alex C. Valach⁷, Dennis Baldocchi⁷, Kyle Delwiche³, Ankur R Desai⁸, Eugenie
 8 Euskirchen⁹, Jinxun Liu¹⁰, Annalea Lohila^{11,12}, Avni Malhotra³, Lulie Melling¹³, William
 9 Riley¹⁴, Benjamin R. K. Runkle¹⁵, Jessica Turner¹⁶, Rodrigo Vargas¹⁷, Qing Zhu¹⁴, Tuula Alto¹²,
 10 Etienne Fluet-Chouinard³, Mathias Goeckede¹⁸, Joe R. Melton¹⁹, Oliver Sonnentag²⁰, Timo
 11 Vesala¹¹, Eric Ward²¹, Zhen Zhang²², Sarah Feron^{3,23}, Zutao Ouyang³, Pavel Alekseychik²⁴,
 12 Mika Aurela¹², Gil Bohrer²⁵, David I. Campbell²⁶, Jiquan Chen²⁷, Housen Chu²⁸, Higo J
 13 Dalmagro²⁹, Jordan P. Goodrich²⁶, Pia Gottschalk³⁰, Takashi Hirano³¹, Hiroki Iwata³², Gerald
 14 Jurasinski³³, Minseok Kang³⁴, Franziska Koebsch³³, Ivan Mammarella¹¹, Mats B. Nilsson³⁵,
 15 Keisuke Ono³⁶, Matthias Peichl³⁵, Olli Peltola¹², Youngryel Ryu³⁷, Torsten Sachs³⁰, Ayaka
 16 Sakabe³⁸, Jed Sparks³⁹, Eeva-Stiina Tuittila⁴⁰, George L Vourlitis⁴¹, Guan Xhuan Wong¹³,
 17 Lisamarie Windham-Myers⁴², Ben Poulter⁴³, Robert B. Jackson^{3,44,45}

18
 19
 20
 21 ¹ Department of Geography, The University of British Columbia, Vancouver, British Columbia,
 22 Canada

23 ² U.S. Geological Survey, Northern Prairie Wildlife Research Center, 8711 37th St Southeast,
 24 Jamestown, ND 58401 USA

25 ³ Department of Earth System Science, Stanford University, Stanford, California

26 ⁴ Department of Earth and Environmental Science, Rutgers University Newark, NJ

27 ⁵ National Ecological Observatory Network, Battelle, Boulder, CO, USA

28 ⁶ Graduate School of Life and Environmental Sciences, Osaka Prefecture University

29 ⁷ Department of Environmental Science, Policy and Management, University of California,
 30 Berkeley, CA, USA

31 ⁸ Dept of Atmospheric and Oceanic Sciences, University of Wisconsin-Madison, Madison, WI
 32 53706 USA

33 ⁹ University of Alaska Fairbanks, Institute of Arctic Biology, Fairbanks, AK, USA

34 ¹⁰ U.S. Geological Survey, Western Geographic Science Center, Moffett Field, CA, USA

35 ¹¹ Institute for Atmospheric and Earth System Research/Physics, Faculty of Science, University
 36 of Helsinki, Helsinki, Finland

37 ¹² Climate System Research, Finnish Meteorological Institute, PO Box 503, 00101 Helsinki,
 38 Finland

39 ¹³ Sarawak Tropical Peat Research Institute, Sarawak, Malaysia

40 ¹⁴ Earth and Environmental Sciences Area, Lawrence Berkeley National Lab, Berkeley,
 41 California

- 42 ¹⁵ Department of Biological & Agricultural Engineering, University of Arkansas, Fayetteville,
43 Arkansas 72701, United States
- 44 ¹⁶ Freshwater and Marine Science, University of Wisconsin-Madison
- 45 ¹⁷ Department of Plant and Soil Sciences, University of Delaware, Newark, DE, USA
- 46 ¹⁸ Department of Biogeochemical Signals, Max Planck Institute for Biogeochemistry, Jena,
47 Germany
- 48 ¹⁹ Climate Research Division, Environment and Climate Change Canada, Victoria, B.C., Canada
- 49 ²⁰ Université de Montréal, Département de géographie, Université de Montréal, Montréal, QC
50 H2V 0B3, Canada
- 51 ²¹ U.S. Geological Survey, Wetland and Aquatic Research Center, Lafayette LA
- 52 ²² Department of Geographical Sciences, University of Maryland, College Park, MD 20740,
53 USA
- 54 ²³ Department of Physics, University of Santiago, Santiago de Chile, Chile
- 55 ²⁴ Natural Resources Institute Finland (LUKE), Latokartanonkaari 9, 00790 Helsinki, Finland
- 56 ²⁵ Department of Civil, Environmental & Geodetic Engineering, Ohio State University
- 57 ²⁶ School of Science, University of Waikato, Hamilton, New Zealand
- 58 ²⁷ Department of Geography, Environment, and Spatial Sciences, & Center for Global Change
59 and Earth Observations, Michigan State University, East Lansing, MI
- 60 ²⁸ Climate and Ecosystem Sciences Division, Lawrence Berkeley National Lab
- 61 ²⁹ Universidade de Cuiaba, Cuiaba, Mato Grosso, Brazil
- 62 ³⁰ GFZ German Research Centre for Geosciences, Telegrafenberg, 14473 Potsdam, Germany
- 63 ³¹ Research Faculty of Agriculture, Hokkaido University
- 64 ³² Department of Environmental Science, Faculty of Science, Shinshu University
- 65 ³³ University of Rostock, Rostock, Germany
- 66 ³⁴ National Center for Agro Meteorology, Seoul 08826, South Korea
- 67 ³⁵ Dept. of Forest Ecology and Management, Swedish University of Agricultural Sciences, 901
68 83 Umeå, Sweden
- 69 ³⁶ Institute for Agro-Environmental Sciences, National Agriculture and Food Research
70 Organization, Tsukuba, Japan
- 71 ³⁷ Department of Landscape Architecture and Rural Systems Engineering, Seoul National
72 University, Seoul 08826, South Korea
- 73 ³⁸ Kyoto University, Kyoto, 606-8502, Japan
- 74 ³⁹ Department of Ecology and Evolutionary Biology, Cornell, Ithaca, NY
- 75 ⁴⁰ School of Forest Sciences, University of Eastern Finland, Joensuu, Finland
- 76 ⁴¹ California State University San Marcos, San Marcos, CA, USA
- 77 ⁴² U.S. Geological Survey, Water Mission Area, 345 Middlefield Road, Menlo Park, CA, 94025
- 78 ⁴³ Biospheric Sciences Laboratory, NASA Goddard Space Flight Center, Greenbelt, Maryland
- 79 ⁴⁴ Woods Institute for the Environment, Stanford University, Stanford, California
- 80 ⁴⁵ Precourt Institute for Energy, Stanford University, Stanford, California

81
82

83 *Corresponding author: Sara H. Knox, Tel: +1 (604) 833-0999; email: sara.knox@ubc.ca

84 **Article type:** Primary Research Articles

85 This draft manuscript is distributed solely for purposes of scientific peer review. Its content is
86 deliberative and predecisional, so it must not be disclosed or released by reviewers. Because the
87 manuscript has not yet been approved for publication by the U.S. Geological Survey (USGS), it
88 does not represent any official USGS finding or policy.

89
90 **Keywords:** Wetlands, methane, eddy covariance, synthesis, predictors, generalized additive
91 modeling, mutual information, random forest, time scales, lags

92

93

94 **Abstract:**

95 While wetlands are the largest natural source of methane (CH₄) to the atmosphere, they represent
96 a large source of uncertainty in the global CH₄ budget due to the complex biogeochemical
97 controls on CH₄ dynamics. Here we present, to our knowledge, the first multi-site synthesis of
98 how predictors of freshwater wetland CH₄ fluxes (FCH₄) vary across wetland types at diel,
99 multiday (synoptic), and seasonal time scales. We used several statistical approaches (correlation
100 analysis, generalized additive modeling, mutual information, random forests) in a wavelet-based
101 multiresolution framework to assess the importance of environmental predictors, nonlinearities
102 and lags on FCH₄ across 23 eddy covariance sites. Seasonally, soil and air temperature were
103 dominant predictors of FCH₄ at sites with smaller seasonal variation in water table depth
104 (WTD). In contrast, WTD was the dominant predictor for wetlands with smaller variations in
105 temperature (e.g., seasonal tropical/subtropical wetlands). Changes in seasonal FCH₄ lagged
106 fluctuations in WTD by $\sim 17 \pm 11$ days, and lagged air and soil temperature by median values of
107 8 ± 16 and 5 ± 15 days, respectively. Temperature and WTD were also dominant predictors at
108 the multiday scale. Atmospheric pressure (PA) was another important multiday scale predictor
109 for peat dominated sites, with drops in PA coinciding with synchronous releases of CH₄. At the
110 diel scale, synchronous relationships with latent heat flux and vapor pressure deficit suggest that
111 physical processes controlling evaporation and boundary layer mixing exert similar controls on
112 CH₄ volatilization, and suggest the influence of pressurized ventilation in aerenchymatous
113 vegetation. In addition, 1-4 hour lagged relationships with ecosystem photosynthesis indicate
114 recent carbon substrates, such as root exudates, may also control FCH₄. By addressing issues of
115 scale, asynchrony, and nonlinearity, this work improves understanding of the predictors and

- 116 timing of wetland FCH₄ that can inform future studies and models, and help constrain wetland
- 117 CH₄ emissions.

118 **1. Introduction**

119

120

121

122

123

124

125

126

127

128

129

130

131

132

133

134

135

136

137

138

139

140

141

Methane (CH₄) is responsible for almost one quarter of the cumulative radiative forcing since the start of the industrial revolution (Etminan et al., 2016). As the largest natural source to the atmosphere, wetlands are responsible for ~30% of global CH₄ emissions, but their contribution to the global CH₄ budget is highly uncertain (Bridgham et al., 2013; Jackson et al., 2020; Saunois et al., 2020). The complexity of wetland CH₄ exchange, which is the net result of CH₄ production, consumption, and transport, makes interpreting and predicting fluxes challenging (Bridgham et al., 2013).

Previous site-level (Chu et al., 2014; Desai et al., 2015; Pugh et al., 2018; Chang et al., 2019) and synthesis studies (Moore & Dalva, 1993; Updegraff et al., 2001; Olefeldt et al., 2013; Turetsky et al., 2014; Treat et al., 2018; Knox et al., 2019; Peltola et al., 2019) of wetland CH₄ exchange have improved understanding of the abiotic and biotic controls on wetland CH₄ fluxes (FCH₄). These studies established that temperature, water table position, air pressure and atmospheric turbulence, sediment biogeochemistry, and vegetation often dominate as coarse controls on net FCH₄ from wetlands, with distinct controls varying by wetland type (Lai, 2009; Bridgham et al., 2013; Olefeldt et al., 2013; Turetsky et al., 2014; Treat et al., 2018; Wen et al., 2018). Both air and soil temperature (TA and TS, respectively) can influence FCH₄, with the former dominating physical processes of diffusive transport in plants and the latter strongly influencing microbial processes controlling CH₄ production and oxidation and subsequent soil diffusion and ebullition; thus, both often emerge as dominant predictors of FCH₄ within and across sites (Knox et al., 2019; Morin, 2019). Water table depth (WTD) governs the reduction-oxidation (redox) zones that determine CH₄ production and oxidation (Moore & Knowles, 1989; Bubier et al., 1995; Malhotra & Roulet, 2015; Perryman et al., 2020, etc.). Physical processes

142 such as turbulent conditions and atmospheric pressure (PA) fluctuations can influence the
143 transport of CH₄ from the soil profile into the atmosphere, particularly in porous peat soils where
144 ebullition is often the primary CH₄ transport mechanism during the pressure-falling phase (Sachs
145 et al., 2008; Nadeau et al., 2013; Ueyama et al., 2020b). Biological factors such as plant
146 community type and primary production also influence CH₄ production and consumption
147 through a variety of mechanisms including: supplying labile carbon compounds that fuel
148 methanogenesis (Christensen et al., 2003; Tittel et al., 2019); enhancing oxygen transport into
149 anoxic soil layers via aerenchyma thereby supporting rhizosphere CH₄ oxidation (Laanbroek,
150 2010); and mediating transport of CH₄ to the atmosphere via aerenchyma, allowing CH₄ to
151 bypass potential oxidation in surface soils (Knoblauch et al., 2015; Kwon et al., 2017; Villa et
152 al., 2020).

153 Determining the environmental controls on FCH₄ is critical for understanding and
154 modeling these fluxes. In addition to considering direct, mechanistic drivers of methanogenesis,
155 methanotrophy and CH₄ transport (e.g., temperature, WTD, PA) (c.f., Table 1), there are also
156 benefits to understanding alternative variables that are strongly correlated with FCH₄ even if
157 such variables (e.g., latent heat (LE)) are indirectly linked to FCH₄ (Table 1). These indirect
158 variables can be measured alongside FCH₄ and its direct drivers to help capture the complex and
159 nonlinear relationships between environmental drivers and FCH₄ and can describe similar
160 processes to those influencing CH₄ exchange (Morin et al., 2014), and therefore are well-suited
161 for inclusion in data-driven FCH₄ models.

162 While a general concept of the overall controls on wetland FCH₄ has been established,
163 understanding the functional controls on FCH₄ is highly influenced by the temporal and spatial
164 scales of measurements (Turetsky et al., 2014). In particular, until recently, data and synthesis

165 studies were largely biased toward chamber-based measurements from temperate and northern
166 high-latitude regions (Olefeldt et al., 2013; Turetsky et al., 2014). However, manual chamber
167 measurements are typically discrete in time and space, and therefore may not capture the full
168 spatiotemporal range of CH₄ dynamics, limiting the investigation of the underlying drivers and
169 patterns of FCH₄ in wetlands (Morin, 2019).

170 Eddy covariance (EC) flux towers provide ecosystem-scale, noninvasive and near-
171 continuous measurements of the exchange of mass (e.g., carbon dioxide (CO₂), CH₄, water) and
172 energy between the land surface and the atmosphere (Baldocchi, 2014). Methane exchange in
173 wetlands often involves nonlinear and asynchronous processes across multiple time scales
174 (Sturtevant et al., 2016; Schaller et al., 2019). The continuous, high-frequency nature of EC
175 measurements along with supporting biophysical measurements offer promising datasets for
176 improving understanding of wetland FCH₄ over multiple timescales. For example, water-level
177 fluctuations correspond with pulses of CH₄ with hourly to daily delays (Hatala et al., 2012a), but
178 also inhibit FCH₄ across a range of time scales (Sturtevant et al., 2016; Koebisch et al., 2015).
179 However, despite the fact that many of these processes and time scales are poorly characterized
180 at the ecosystem scale, they are important for predicting FCH₄ and, therefore, are critical to
181 include in data-driven and process-based models (Koebisch et al., 2015; Li et al., 2018). While
182 studies using EC flux data can elucidate these knowledge gaps, most studies focus on single
183 sites, thus limiting the scope of inference and generalization across multiple wetland types at
184 regional and global scales. Furthermore, given the complexity of wetland FCH₄, more studies
185 explicitly questioning assumptions of linear, synchronous, and single-scale analyses are needed,
186 which can provide new insights into interpretations and predictions of CH₄ dynamics.

187 Robust statistical approaches are required to capture and describe CH₄ dynamics.
188 Numerous statistical methods with known strengths and weaknesses have been used to describe
189 and model FCH₄, ranging from simple correlation analysis to more complex machine-learning
190 algorithms (Genuer et al., 2010; Peltola et al., 2019; Kim et al., 2020). By implementing and
191 comparing multiple statistical approaches, it is possible to evaluate how our understanding of the
192 complex interactions between controls on FCH₄ is influenced by the choice of statistical analysis
193 (Trifunovic et al., 2020).

194 In this study, we take advantage of near-continuous EC measurements to elucidate the
195 predictors and timing of wetland CH₄ flux dynamics. Here we use the term ‘predictor’ rather
196 than ‘driver’ or ‘control’ since we are considering direct, indirect and coincident variables
197 associated with FCH₄ (c.f., Table 1). We leverage the FLUXNET-CH₄ dataset (Knox et al.,
198 2019; Delwiche et al., in review) and multiple statistical approaches to analyze measurements
199 from 23 EC sites across the world (representing 107 site-years of data) to better constrain the
200 dominant predictors of freshwater, non-tidal wetland FCH₄ across time scales and wetland types.
201 Specifically, we address the following questions: i) What are the dominant predictors of FCH₄ at
202 diurnal to seasonal time scales at each wetland? ii) How does the relative dominance of each
203 predictor vary across wetland types? iii) Is the identification of dominant predictors of FCH₄
204 influenced by the choice of statistical approach? iv) How important are nonlinearities and lags in
205 interpreting FCH₄?

206 **2. Methods**

207

208 *2.1. Dataset and site description*

209

210 Twenty-three sites from the FLUXNET-CH₄ database (Table 2, Fig. 1) were selected for
211 this analysis because they had at least one full year of FCH₄ measurements and reported all

212 predictors of interest (Table 1). We only analyzed data for non-tidal, freshwater wetlands
213 because FCH₄ from tidal wetlands is influenced by additional factors such as salinity, sulfate
214 reduction, and tidal action (Seyfferth et al., 2020). Data standardization, gap-filling, and
215 partitioning of net ecosystem exchange (NEE) of CO₂ for the FLUXNET-CH₄ dataset are
216 described in detail in Knox et al. (2019) and Delwiche et al. (in review). Here we considered
217 physical predictors of FCH₄ such as TA, TS, WTD, PA, incoming shortwave radiation (SW_IN),
218 vapor pressure deficit (VPD), and wind direction (WD), biological predictors such as gross
219 primary productivity (GPP), NEE, or ecosystem respiration (RECO), and coincident, indirect
220 variables such as LE, to understand which variables are strongly correlated with FCH₄ and under
221 what conditions and time scales (Table 1). When more than one observation depth for TS was
222 available, we selected TS at the depth where the statistical dependence of FCH₄ on TS was
223 highest (see Section 2.2.3). As noted above, here we use the term ‘predictor’ rather than the
224 terms ‘driver’ or ‘control’ since several of the variables considered here do not have a direct
225 influence on CH₄ production, consumption and/or transport, but rather reflect variables that
226 represent a proxy or are correlated with processes that have a direct influence on FCH₄.
227 However, in the Discussion we emphasize which predictors represent direct drivers of FCH₄ and
228 which reflect proxies (c.f., Table 1).

229 Sites were classified into bog, fen, marsh, swamp, rice paddy, and drained wetland based
230 on site-specific literature (Delwiche et al., in review) (Table 2, Fig. 1). Climate was extracted and
231 modified from Olson et al. (2001) using site coordinates and includes boreal, temperate, and
232 tropical/subtropical. No tundra sites were included in this analysis due to the lack of key
233 ancillary variables (e.g., WTD) in the FLUXNET-CH₄ database. Management regimes included
234 natural, managed, and restored freshwater wetlands (Table 2).

235 *2.2. Within-site analysis of the dominant predictors of CH₄ fluxes*

236 To investigate the complexity of wetland FCH₄, we compared multiple statistical
237 approaches to analyze the dominant predictors of FCH₄ and evaluate whether findings of the
238 most important predictors of FCH₄ were consistent across approaches. We used methods
239 commonly used in analyses of FCH₄ and their drivers, ranging from simple linear correlation to
240 more complex methods such as generalized additive models (GAM), information theory, and
241 random forests (RF). For each method, the goal was to identify and rank the importance of
242 predictors of FCH₄ (i.e., independent variables) to explain the variability of FCH₄ (i.e.,
243 dependent variable).

244 Variable importance analyses using each of the four methods were first performed using
245 daily mean data, a common time step for analyzing FCH₄ (Turetsky et al., 2014; Rinne et al.,
246 2018). Analyses were also performed on wavelet-decomposed data using half-hourly data, as
247 described below, to assess how predictors vary across time scales (i.e., diel to seasonal time
248 scales), as partitioning variability across scales can help isolate and identify important processes
249 (Koebsch et al., 2015).

250 *2.2.1. Wavelet-based time-scale decomposition*

251 The maximal overlap discrete wavelet transform (MODWT) was used to decompose the
252 time scales of variability in gap-filled FCH₄ and explanatory variables (Sturtevant et al., 2016)
253 (see Supporting Information for full details and implementation including treatment of gaps).
254 The MODWT decomposes the time series into the detail added from progressively coarser to
255 finer scales, and can be either summed or treated individually to explore patterns across scales.
256 The detail in the half-hourly fluxes were reconstructed for dyadic scales 1 (2^1 measurements = 1
257 h) to 14 (2^{14} measurements = 341 days). We summed the detail over adjacent scales to yield four

258 general time scales of variation (Sturtevant et al., 2016). Time scales of variation included the
259 “hourly scale” (1–2 h) representing short-term perturbations such as clouds passing overhead, the
260 “diel scale” (4 h to 1.3 days) representing the diel cycles in radiation and temperature, the
261 “multiday scale” (2.7 to 21.3 days) encompassing synoptic weather variability and shorter-term
262 variations in water levels, and the “seasonal scale” (42.7 to 341 days) representing vegetation
263 phenology, seasonal hydrological cycle, and the annual solar cycle. Data were wavelet
264 decomposed into the hourly, diel, multiday, and seasonal scales with the Wavelet Methods for
265 Time Series Analysis (WMTSA) using the Wavelet Toolkit in MATLAB (Cornish et al., 2003).
266 We focused predominantly on the predictors of diel to seasonal time scales as the hourly wavelet
267 scale is often dominated by noise (Hollinger & Richardson, 2005). As such, the hourly scale was
268 only produced to show the distribution of FCH₄ variability across time scales.

269 Since wavelet decomposition requires special treatment of gaps, we used gap-filled data
270 from the FLUXNET-CH₄ database for the wavelet decomposition. However, following wavelet
271 decomposition, the original gaps were subsequently re-introduced prior to the analyses described
272 below in all but the seasonal time scale to minimize biasing the results based on gap-filling
273 algorithms (Sturtevant et al., 2016). Original gaps at the seasonal scale were not removed
274 because gap lengths were small relative to this scale.

275 2.2.2. *Linear correlation*

276 A pairwise Pearson’s linear correlation analysis between predictors and FCH₄ was
277 performed on all sites and time scales described above, with predictor importance represented by
278 the coefficient of determination (Table S1). Log transformation was not performed as difficulties
279 arise in interpreting log transformed variables. In addition, negative and zero values would need
280 to be either discarded or manipulated for a log transformation and therefore skew the results. All
281

282 analyses were conducted in Matlab 2019a (Mathwork Inc., Natick, MA, USA). The linear
283 correlation was deemed significant at an α level of 0.05.

284 2.2.3. *Relative Mutual Information (IR)*

285
286 In information theory, mutual information (I), defines the average tendency for paired
287 states of two variables (e.g., X and Y) to coexist (Fraser & Swinney, 1986). Computed from the
288 marginal and joint probability distributions of X and Y, relative mutual information (IR_{XY})
289 characterizes the proportion of bits required to represent Y that is redundant given the knowledge
290 of X. Put differently, it is a normalized measure of the statistical dependence of Y on X, with
291 larger values indicating higher dependence, or in this context, identifying a stronger link to
292 FCH4. A strength of I_{XY} lies in the lack of parametric assumptions about the relationships
293 between X and Y, and therefore, it can address both linear and nonlinear interactions. The
294 strength of I_{XY} and IR_{XY} is further enhanced by adding a time lag (τ) to these metrics, thereby
295 allowing us to identify both synchronous and asynchronous interactions. A “synchronous”
296 interaction is defined as one in which the maximum IR_{XY} is found at $\tau = 0$ (i.e., zero-time lag),
297 indicating that variations in Y are most related to simultaneous variations in X. Otherwise, the
298 interaction is characterized as “asynchronous”, where maximum IR_{XY} at $\tau > 0$ indicates that the
299 fluctuations in Y lagged variations in X, while maximum IR_{XY} at $\tau < 0$ implies that variations in
300 Y lead variations in X. As such, mutual information can identify both the statistical strength (i.e.,
301 predictor importance) and asynchrony of complex biosphere-atmosphere interactions, such as
302 wetland FCH4 (Sturtevant et al., 2016).

303 IR between FCH4 (X) and biophysical predictors (Y) of interest was calculated for both
304 daily mean data and wavelet decomposed data over a range of time lags (τ) using version 1.5 of
305 the ProcessNetwork Software (Table S2) (Ruddell et al., 2008). Details on the lags,

306 discretization, statistical significance and bias correction are provided in the Supporting
307 Information.

308 2.2.4. *Generalized additive models (GAMs)*

309
310 The third method used to assess important predictors of FCH₄ were GAMs. FCH₄ often
311 follows nonlinear relationships with various potential predictor variables. Unlike linear
312 correlation analysis, GAMs have the capability of describing these nonlinear relationships and
313 treating the degree of nonlinearity as a quantity to be estimated. We developed GAMs of FCH₄
314 using each predictor individually. Relative predictor importance was determined by comparing
315 the deviance explained among predictors (Table S3). All GAMs were implemented using the
316 *mgcv* package in R version 3.6.2 (Wood, 2011), with details provided in the Supporting
317 Information.

318 2.2.5. *Random forests (RF)*

319 The last method used to assess variable importance and the dominant predictors of FCH₄
320 was random forests (RF), which is a machine learning algorithm that grows an ensemble of
321 decision trees (Breiman, 2001). A strength of decision trees is that this approach can reproduce
322 nonlinearities among multiple predictor variables to explain FCH₄. For each tree, data are
323 successively split at decision nodes to minimize variance in the resulting branches. Predictor
324 variables can be considered at multiple decision nodes within a single tree, allowing the RF
325 algorithm to thoroughly explore possible predictor conditions. Moreover, the RF algorithm is
326 less prone to issues of overfitting associated with single trees because it grows an ensemble
327 (forest) of decision trees and each tree is trained using randomly drawn (bagged) subsamples of
328 the data.

329 A RF algorithm was trained for each site using the *ranger* package in R (Wright &
330 Ziegler, 2017; R Core Team, 2019) with details provided in the Supporting Information. We
331 ranked predictors using permutation importance, which avoids bias of other methods (Strobl et
332 al., 2007) and scaled importances for site comparisons (Table S4). We also provide out-of-bag
333 model fit metrics (coefficient of determination, mean absolute error, and bias) as a further
334 evaluation of relative confidence in results between sites (Fig. S13, Fig. S14).

335 2.2.6. Variable importance standardization

336 Each statistical method was used to provide a numeric ranking of variable importance,
337 which we used to estimate dominant FCH₄ predictors (i.e., the highest ranked covariates) and
338 assess how predictors vary between statistical methods. However, the statistical approaches have
339 different scales for variable importance scores and different ranges between sites. As such,
340 variable importance metrics for each method were normalized between zero and one, and
341 therefore for all sites and methods, the strongest predictor has a value of one and the lowest a
342 value of zero. This normalization ensures comparability in scores across wetland sites and
343 methods.

344 2.3. Visualizing and cross-site synthesis of the dominant predictors of CH₄ fluxes

345 To distill the information generated from the variable importance metrics described
346 above, heatmaps and principal component analysis (PCA) were used to visualize and assess
347 predictor patterns across sites and wetland types. Here we used the *heatmap.2* function in *gplots*
348 R package (Warnes et al., 2019) to generate a heatmap (without cluster analysis) of the
349 normalized variable importance metrics described above to help visualize dominant predictors
350 across sites.

351 PCA analysis was used to summarize and visualize the information contained in the
352 variable importance analysis. For each method, we compressed the standardized variable
353 importance scores generated using the statistical approaches described in Sections 2.2.2-2.2.5
354 into two principal components. The distributions of sites on the principal components visualize
355 how strongly FCH₄ at each site was regulated by the environmental predictors. PCA analysis
356 was done using the *prcomp* function in base R. Columns of the normalized matrices were
357 centered so that the mean of each column was equal to zero (Abdi & Williams, 2010).

358 **3. Results**

359 *3.1. Magnitude of FCH₄ and time scales of variability*

360 FCH₄ exhibited a wide range of magnitude across the 23 sites, with median FCH₄ varying
361 from 0.5 to 541 nmol m⁻² s⁻¹ (Table 2). Median FCH₄ averaged within wetland types was highest
362 in marshes, followed by rice, fens, bogs, and swamps.

363 FCH₄ exhibited strong variation across time scales (Fig. 2). The seasonal time scale tended
364 to dominate FCH₄ variability across wetland sites, although it was notably lower in some
365 tropical/subtropical sites where the seasonal variability of multiple biophysical predictors (e.g.,
366 radiation, temperature, GPP) tended to be much lower than in temperate and boreal sites. The
367 variation in FCH₄ at multiday and hourly scales was generally low. However, some sites with
368 low fluxes tended to have higher variation at the hourly scale (e.g., FI-Si2 and US-Uaf) due to
369 the higher signal to noise ratio (Hollinger & Richardson, 2005).

370 Variation at the diel scale also varied across sites. Sites with high diel FCH₄ variation
371 typically showed a diurnal pattern of highest fluxes during late-morning to mid-afternoon and
372 lower fluxes at night (Fig. 2, Fig. S1). Nonetheless, some sites with considerable variation at the
373 diel scale exhibited different diurnal patterns (Fig. S1). At some sites, the proportion of variance

374 in FCH4 at the diel scale appeared large despite a lack of a typical diurnal pattern (e.g., ID-Pag,
375 FI-Si2, MY-MLM, US-Uaf). This was largely attributed to the fact that at these sites variation at
376 other scales (e.g., seasonal) was low (Fig. 2) and/or the magnitude of FCH4 was low (Table 2).

377 *3.2. Dominant predictors of FCH4 across time scales*

378 *3.2.1. Summary across sites, time scales and methods*

379 To assess the dominant predictors at each time scale, we averaged normalized variable
380 importance scores across sites for each method (Table 3). At the seasonal scale, TS always
381 ranked as the dominant predictor. TA alternated as either the second or third most important
382 predictor along with LE or NEE. Overall, the different approaches tended to converge on the top
383 predictors, with each of these dominant predictors explaining on average >50% of the variance in
384 seasonal FCH4 based on the linear correlation and GAM analyses (Tables S1 and S3).

385 Similar to the seasonal scale, there was also general consistency between methods at the
386 multiday scale, with all approaches again identifying temperature (TS and/or TA) in the top three
387 predictors (Table 3). Other key predictors that emerged at the multiday scale included PA, LE,
388 WTD, and wind direction (WD). While overall less of the variability in multiday FCH4 was
389 explained by each of the individual predictors, the top predictor at each site generally explained
390 between 10 and 50% of the variance in multiday FCH4 (Table S1 and S3), with site-level $R^2 >$
391 0.95 for the RF model with all predictors (Fig. S13).

392 At the diel scale, all approaches identified LE and NEE as the top two predictors of FCH4,
393 and with GPP or SW_IN as the third most important predictor depending on the method (Table
394 3). While the explanatory power of individual predictors was lowest at the diel scale, predictors
395 did explain up to 50% of the variability in FCH4 for sites with a typical diurnal pattern (i.e.,
396 lower fluxes at night and higher during the day) (Table S1 and S3).

397 Daily averaged data are often used for analysis of FCH₄ variation at the seasonal scale (Chu
398 et al., 2014; Rinne et al., 2018). However, unlike wavelet seasonal transformed data, daily
399 averages also include influences from other time scales of variation. As such, although
400 temperature (TS or TA) was consistently found to be the top driver across methods at this time
401 step, other variables such as GPP, NEE and WTD, which were identified as key controls of
402 FCH₄ at the multiday and diel scales, were also identified in the top three drivers for daily
403 averaged data (Table 3).

404 Given the consistent patterns across methods (Table 3), we focus on the findings of the IR
405 method for the remainder of the results. The IR approach is explicitly designed to identify both
406 synchronous and asynchronous relationships (Sturtevant et al., 2016), representing an advantage
407 over the other statistical methods where accounting for lags is possible but it is not among their
408 inherent strengths. However, results from the other statistical approaches are presented as
409 necessary (primarily in the SI) to show consistency or highlight differences in the methods.

410 3.2.2. *Patterns within and across sites at the seasonal scale*

411 Figure 3 shows a detailed picture of the dominant predictors within and across sites
412 determined by maximum IR between FCH₄ and biophysical variables. The heatmap at the
413 seasonal scale for both maximum IR (Fig. 3a) and synchronous IR (Fig. S2a) shows that
414 temperature (TS or TA) was the dominant predictor across the majority of sites at this scale, with
415 LE, NEE, and GPP also among top predictors, corroborating the broader patterns across sites
416 shown in Table 3. The dominance of temperature, LE, NEE, and GPP was also apparent in the
417 other statistical approaches (Fig. S3). However, Fig. 3a and Fig. S2a also revealed other patterns
418 which were obscured when averaging variable rankings across sites; notably, WTD was a

419 dominant predictor at the swamp and drained sites and two of the rice paddy sites. The
420 importance of WTD at these sites was also consistent across statistical methods (Fig. S3).

421 The importance of temperature and WTD was also evident in the PCA analysis of IR
422 results (Fig. 4). Sites clustered along PC1 (29% of explained variance) which corresponds
423 predominantly with WTD, TA, LE and VPD (highly correlated with TA) as dominant predictors
424 of FCH₄ at the seasonal scale (Table S5). This clustering by wetland type further supports the
425 finding above that, while temperature was a dominant predictor at most sites, WTD was a key
426 control at the swamp, drained but seasonally inundated, and two of the rice paddy sites. Sites
427 where WTD is a dominant predictor at the seasonal scale also tended to have a greater ratio in
428 the variation of WTD relative to TA (Fig. 4). This visible clustering along axes of WTD and
429 temperature (and variables correlated with temperature) was also apparent in the PCA analysis of
430 the results from the linear correlation, GAM, and RF analyses (Fig. S4), again supporting the
431 findings of the IR analysis of the dominant predictors of FCH₄ at the seasonal scale (Table 3,
432 Fig.S3, Fig. S4).

433 The results of the PCA analysis also suggested other clusters across wetland types. Fens
434 and most bogs tended to cluster together along PC2 in the bottom right corner of the scatter plot
435 indicating the importance of GPP and RECO as secondary predictors of FCH₄ in these wetland
436 types (Fig. 4, Fig. 3a, Table S5). However, except for GAM, similar clustering for bogs and fens
437 was less apparent in the other statistical approaches (Fig. S4).

438 For sites where WTD was among the higher ranked predictors (the swamp and drained
439 sites, two rice paddy sites, and the bog NZ-Kop; Fig. S6), seasonal FCH₄ lagged WTD by an
440 average of approximately 17 ± 11 days (standard deviation) (Fig. 5a, Fig. S5, Fig. S6). The lag at
441 peak IR_{WTD, FCH_4} at individual sites ranged from 2 to 35 days (Fig.5a, Fig. S5, Fig. S6). The

442 median lag between seasonal FCH₄ and TA was 8 ± 16 days (Fig. 5b), and the median lag with
443 TS was 5 ± 15 days (Fig. 5c). These findings suggest a more synchronous relationship between
444 FCH₄ and temperature at the seasonal scale relative to WTD (Fig. 5). As noted in the methods,
445 here we selected TS at the depth where IR_{TS,FCH_4} was greatest. We hypothesize this is the depth
446 where CH₄ production was greatest but acknowledge the lack of information on the depth profile
447 of CH₄ oxidation and labile carbon supply. With respect to negative lags with TS, a negative lag
448 does not indicate that seasonal FCH₄ began to increase before TS; for all sites and site years,
449 seasonal FCH₄ began to increase after TS, and therefore negative lags with TS reflected the fact
450 that seasonal FCH₄ peaked prior to TS and/or began to decrease prior to the decrease in TS at the
451 end of the growing season (Fig. S7). Lags were also observed with respect to other top predictors
452 of seasonal FCH₄ (Fig. 5d,e), where both LE and GPP tended to increase and/or peak prior to
453 FCH₄ (Fig. S8). The median lag between FCH₄ and LE was 17 ± 18 days (Fig. 5d), while FCH₄
454 lagged GPP by 12.5 ± 23 days (Fig. 5e).

455 3.2.3. *Patterns within and across sites at the multiday scale*

456
457 WTD, TA, and PA were among the top predictors at the multiday scale (Table 3, Table
458 S6, Fig. 3b, Fig. 4b) and were generally consistent across statistical approaches. However, the
459 relationships with WTD and PA were less apparent for linear correlation analysis and GAMs,
460 respectively (Table S6, Fig. S9). While clustering across wetland types was less pronounced at
461 the multiday scale (Fig. 4b, Fig. S10), some patterns emerged. Notably, PA was in the top three
462 predictors at several peat-dominated sites, including bogs, fens, a peat swamp, and a restored
463 marsh underlain by peat (Fig. 3a, Fig. S10). The relationship between FCH₄ and PA was near-
464 synchronous. Although Fig. 6a suggests that FCH₄ slightly led drops in PA (on the order of $\sim 4 \pm$
465 2 hours), these lags are not significantly different from zero at the multiday scale (Sturtevant et

466 al., 2016). As such, drops in PA coincided with synchronous releases of FCH₄ (Fig. 6b, Fig.
467 S10). Pressure fluctuations on the order of 0.5 to 2 kPa resulted in pulses of CH₄ on the order of
468 5 to 100 nmol m⁻² s⁻¹, with larger pulses in CH₄ at high emitting sites (Fig. S10).

469 Similar to the relationship with PA, there was a near-synchronous relationship between
470 multiday temperature (both TA and TS) and FCH₄ (Fig. 6c). WTD was also one of the top
471 predictors at several sites (Fig. 3b, Fig. 4b, Fig S9) but had a slightly more complex, nonlinear
472 relationship than those described previously at the multiday scale. Examination of IR_{WTD,FCH₄}
473 with lag (Fig. 6e) generally showed both a primary interaction where variation in FCH₄ slightly
474 led variation in WTD (a lag of ~8 hours), and a secondary interaction where FCH₄ lagged WTD.
475 As illustrated for US-Tw1, the wavelet detail reconstruction for these variables (Fig. 6f) showed
476 pulses in CH₄ generally coinciding or occurring slightly before minima in WTD. There also
477 tended to be a secondary peak in IR_{WTD,FCH₄} on the order of 4-6 days (Fig. 6e). This secondary
478 lagged interaction was frequently the result of lower FCH₄ after a subsequent rise in WTD (Fig.
479 6f). The one exception to this pattern was at the rice paddy site (US-Twt), where IR as a function
480 of lag only had a single peak (Fig. 6e), with maximum IR_{WTD,FCH₄} occurring at a lag of ~5 days.

481 3.2.4. *Patterns within and across sites at the diel scale*

482 Some sites had more variation at the diel scale than others. Sites which exhibited a typical
483 diurnal pattern primarily included fens, marshes, swamps, and rice paddies, with amplitudes in
484 the diel pattern ranging between ~8 to 172 nmol m⁻² s⁻¹ (Fig. 7, Fig. S1). While not all fens,
485 marshes, and swamps exhibited diel variation, only one of the bogs had a typical diurnal pattern
486 (Fig. 7, Table 2). All sites with a typical diurnal pattern had aerenchymatous vegetation and only
487 JP-BBY had mosses (*Sphagnum*) present.

488 Across statistical methods, top predictors of FCH₄ at the diel scale included LE, NEE,
489 GPP, although in some cases SW_IN and VPD were also among the top predictors of diel FCH₄
490 (Table 3). Of the sites characterized by a typical diurnal pattern the dominant relationship
491 observed were between FCH₄ and LE (5 sites), GPP (3 sites), net ecosystem production (NEP, or
492 negative NEE) (2 sites), VPD (1 site), and SW_IN (1 site) (Fig. 7). The relationship between
493 FCH₄ and LE was approximately synchronous ($\tau \sim 0$ hours), with lags ranging between -1 and
494 0.5 hours, and a median lag of 0 hours. Lags were slightly longer for the other biophysical
495 predictors, ranging up to 4 hours for GPP, 3 hours for NEP, 2 hours for SW_IN and 1 hour for
496 VPD.

497 While in most cases the mean diel pattern of the biophysical predictor with maximum IR
498 closely matched that of FCH₄, in some cases the diel patterns were less well aligned (e.g., DE-
499 Zrk) (Fig. 7). This discrepancy occurs because IR reflects not only similarity in the shape of the
500 diel pattern, but also in the magnitude of the diel variability (Fig. S11) (Sturtevant et al., 2016).
501 For example, at DE-Zrk, the shape of the diel pattern in FCH₄ appears to be more strongly
502 related to VPD while the amplitude of the pattern was more closely related to GPP (Fig. S11).
503 This discrepancy between the mean diel pattern of the biophysical predictor with maximum IR
504 and FCH₄ was observed in some other sites as well (e.g., KR-CRK; US-Twt); however, when
505 considering synchronous relationships (i.e., $\tau = 0$), in most cases the diel pattern in FCH₄
506 closely matched that of LE or VPD (Fig. S12).

507 **4. Discussion**

508 Methane exchange in wetlands is complex, and often involves nonlinear and lagged
509 interactions across a range of time scales (Sturtevant et al., 2016). While several studies have
510 explored environmental controls on FCH₄ across wetland types and biomes (Olefeldt et al.,

511 2013; Turetsky et al., 2014; Treat et al., 2018), this is the first multi-site synthesis study that
512 explores how predictors of non-tidal, freshwater wetland FCH₄ vary across time scales, assesses
513 how the relative dominance of these predictors vary across wetland types, and identifies
514 nonlinear and asynchronous characteristics of these relationships.

515 *4.1. Comparison of approaches*

516 A unique feature of this study is the use of multiple statistical approaches, ranging from
517 simple (linear correlation) to more complex (GAM, IR, RF), to investigate if our understanding
518 of the predictor FCH₄ relationships are influenced by the method of analysis. All statistical
519 approaches generally converged on the top predictors of FCH₄ across sites and time scales
520 (Table 3). However, when considering patterns and clustering across sites, there were some
521 differences between approaches, most notably at the multiday scale (Fig. S9). For example, at the
522 multiday scale, linear correlation did not identify WTD among the top predictors (Fig. S9). The
523 lack of agreement between linear correlation and IR is similar to a previous study that combined
524 wavelet analysis and IR to investigate site-level FCH₄ (Sturtevant et al., 2016). They found that,
525 while linear correlation analysis was generally capable of capturing the major diel and seasonal
526 relationships, multiday and asynchronous relationships were unresolved using linear correlation
527 (Sturtevant et al., 2016). Therefore, more complex approaches such as IR, GAM and RF may be
528 better suited for investigating complex CH₄ dynamics in wetlands.

529 *4.2. Dynamics of CH₄ exchange and influence of temperature on FCH₄*

530 As observed previously (Knox et al., 2019; Sturtevant et al., 2016), the seasonal time
531 scale tended to dominate FCH₄ variability across sites. The notable exceptions were some
532 tropical and subtropical sites which is expected since they typically do not experience the large

533 seasonal variations in temperature, radiation, and GPP that contribute to the FCH₄ seasonality
534 observed at higher latitude sites (Delwiche et al., in review).

535 Across all statistical methods, temperature (TS or TA) was a dominant predictor of FCH₄
536 at the seasonal scale (Table 3, Fig. 8). This finding agrees with other studies across a range of
537 temperate and boreal wetland ecosystems that identified TS as the dominant control over wetland
538 FCH₄ (Sachs et al., 2008; Chu et al., 2014; Turetsky et al., 2014; Knox et al., 2019; Morin,
539 2019). This relationship is expected because microbial activity is stimulated by increased
540 temperature when there is no water limitation and the seasonal temperature variation is relatively
541 large (Table 1) (Yvon-Durocher et al., 2014). However, the dominance of temperature as a driver
542 of seasonal FCH₄ in this study and earlier studies is influenced by the bias of a larger number of
543 sites located at higher latitudes which exhibit a distinct seasonal pattern in temperature. As
544 discussed below, FCH₄ in seasonally-inundated wetlands, particularly those at lower latitudes
545 with relatively uniform year-round temperature, were strongly influenced by WTD (Fig. 3, Fig.
546 4).

547 Across sites, lags between FCH₄ and temperature at the seasonal scale were
548 predominantly positive, with a median lag of 8 ± 16 days for TA and 5 ± 15 days for TS (Fig. 5,
549 Fig. 8). These positive lags are generally consistent with results from a synthesis of FCH₄
550 seasonality in freshwater wetlands of the FLUXNET-CH₄ dataset that found the spring onset of
551 FCH₄ lags the increase in TS by an average of 31 ± 40 days (Delwiche et al., in review).
552 However, the shorter median lags in this study can be explained by the fact that there was a
553 wider range in lags observed in the FLUXNET-CH₄ dataset (Delwiche et al., in review).
554 Moreover, the lags in this study reflect the alignment between the FCH₄ and TS seasonal
555 wavelet detail which resulted in the highest IR (i.e., the lag reflects the best alignment of the

556 variability in the two timeseries and therefore greatest statistical dependence), rather than reflect
557 the numbers of days FCH₄ lagged the spring increase in temperature. In the fewer instances
558 where we did observe negative lags between FCH₄ and temperature, FCH₄ peaked slightly
559 before TS or TA. This is also consistent with the findings of Delwiche et al. (in review) who
560 observed that for 36% of the wetland sites in the FLUXNET-CH₄ database, the timing of peak
561 seasonal FCH₄ led the soil temperature peak, and the findings of (Chang et al., 2021) who
562 observed a negative seasonal FCH₄ hysteresis with temperature (for both the shallowest and
563 deepest TS used) at a number of sites. However, as discussed in Section 4.6, further research is
564 needed to better mechanistically constrain the causes of the observed lags, in particular for
565 factors affecting CH₄ production, oxidation, and transport (Chang et al., 2019).

566 Across multiple sites, including a range of wetland types, temperature was also a
567 dominant predictor at the multiday scale, with synoptic variations in temperature coinciding with
568 near-synchronous fluctuations in FCH₄ (Fig. 6, Fig. 8). While this pattern can be in part related
569 to changes in CH₄ production with temperature (Yvon-Durocher et al., 2014), changes in
570 temperature can also influence ebullition rates and diffusive fluxes in wetlands through changes
571 in CH₄ solubility, thermal expansion and contraction of free-phase gas, and the transfer of gas
572 across the air-water interface (Table 1) (Barber et al., 1988; Chanton et al., 1989; Fechner-Levy
573 & Hemond, 1996; McNicol et al., 2017).

574 4.3. *Influence of water table dynamics on CH₄ exchange*

575 Coupling wavelet analysis with IR identified nonlinear responses of FCH₄ to WTD
576 across multiple time scales (Fig.8). At the seasonal scale, WTD was the dominant driver of
577 FCH₄ in wetland types and regions with pronounced seasonal variations in WTD and lower
578 variations in temperature (e.g., in seasonal wetlands and rice paddies; Bansal et al. 2018; Runkle

579 et al. 2019) (Fig. 3, Fig. 4). For sites where WTD was a major predictor at the seasonal scale,
580 FCH₄ lagged WTD on the order of 17 ± 11 days (Fig. 5). Lags reported here are within the range
581 reported by other studies that found that FCH₄ lagged WTD by approximately 10-11 days
582 (Moore & Dalva, 1993; Schäfer et al., 2014; Goodrich et al., 2015). Water table fluctuations also
583 modulated FCH₄ at shorter time scales (Fig. 4). Notably, sites with fluctuating water levels
584 tended to show pulses in FCH₄ coinciding or occurring slightly before minimums in WTD,
585 followed by a recovery in FCH₄ with a lag of ~4-6 days following rising water levels (Fig. 6).
586 This result is similar to other studies which have also found FCH₄ pulses during water table
587 drawdown (Moore & Dalva, 1993; Hatala et al., 2012b; Knox et al., 2016; Sturtevant et al.,
588 2016; Bansal et al., 2020). These interactions are consistent with the release of stored CH₄ as
589 hydrostatic pressure drops, with peak release occurring as the water table crosses the soil surface
590 (Knox et al., 2016; Chen et al., 2017; Ueyama et al., 2020b). As illustrated in Fig. 6f, different
591 magnitudes of FCH₄ pulses are therefore likely dependent on the current CH₄ pool in porewater
592 and CH₄ production rates (Sturtevant et al., 2016; Bansal et al., 2020). Furthermore, sustained
593 reduction in FCH₄ following rises in water levels likely result from the time taken to deplete
594 reoxidized alternative electron acceptors or replenish the soil CH₄ pool, causing a slow return to
595 higher CH₄ fluxes (Moore & Dalva, 1993; Sturtevant et al., 2016; Koebisch et al., 2020a). This
596 mechanism can also explain the delay in the rise in FCH₄ following the rise in WTD at the
597 seasonal scale, which is consistent with studies that show recovery time of FCH₄ from weeks to
598 months following re-wetting (Table 1) (Kim et al., 2012).

599 While saturated conditions are generally a prerequisite for CH₄ production (Bridgham et
600 al., 2013), although not exclusively (Angle et al., 2017), WTD did not appear as an important
601 predictor for sites exhibiting relatively low variation in WTD (Fig. 4). This is similar to other

602 studies of wetland CH₄ exchange where the water table remained above the surface or showed
603 little variation (Song et al., 2011; Strachan et al., 2015; Knox et al., 2016; Yang et al., 2017).
604 This result highlights the limitation of these types of observational studies to identify controls
605 that do not vary, and underscores the need for experimental studies and long-term continuous
606 measurements of ecosystem-scale FCH₄ to capture a wide range of environmental conditions
607 (Sturtevant et al., 2016).

608 *4.4. Role of pressure fluctuations on CH₄ exchange*

609 Atmospheric pressure is often observed to be an important control on FCH₄ from
610 peatlands, with ebullition being the main transport mechanisms during the pressure-falling phase
611 (Table 1) (Tokida, 2005; Tokida et al., 2007; Sachs et al., 2008; Nadeau et al., 2013). Decreasing
612 PA can lead to gas release from solution and the enlargement of the volume of gas, resulting in
613 increased ebullition (Tokida et al., 2007). Similarly, in freshwater lake environments, a
614 correlation between low PA and increased rates of FCH₄ is frequently observed (Mattson &
615 Likens, 1990; Casper et al., 2000; Engle & Melack, 2000). We found that PA was a dominant
616 predictor on FCH₄ in several peat dominated sites across a range of wetland types (Fig. 4, Fig.
617 8). As in other studies (Nadeau et al., 2013), we found that drops in PA coincided with
618 synchronous releases of CH₄, with synoptic variations in PA resulting in CH₄ pulses on the order
619 of 5 to 100 nmol m⁻² s⁻¹ (Fig. S10).

620 *4.5. Influence of plant activity on FCH₄ and the relationship between LE and FCH₄*

621 At the seasonal scale, LE, GPP and NEE were generally found to be secondary predictors
622 of FCH₄ (Table 3, Fig. 8). While LE does not directly drive FCH₄, the few studies that have
623 examined the relationship between FCH₄ and LE have always found it to be significant (Morin
624 et al., 2014; Sturtevant et al., 2016; Morin, 2019). This strong association between LE and FCH₄

625 is due to the fact that evaporation of water and CH₄ volatilization from water and plant surfaces
626 are driven by similar physical mechanisms and therefore tend to covary (Table 1) (Morin, 2019).
627 LE is also linked to plant activity (e.g., Leaf Area Index (LAI) is a strong determinant of LE) at
628 the seasonal scale, and hence LE can represent a proxy for CH₄ transport through
629 aerenchymatous vegetation (Table 1) (Morin et al., 2014; Morin, 2019).

630 GPP represents a proxy for the mechanisms of carbon inputs and root exudates to fuel
631 methanogenesis, plant-mediated transport of CH₄ to the atmosphere via aerenchymatous tissue,
632 and oxygen transport via aerenchyma into the soil fuel methane oxidation and/or reduce methane
633 production (Table 1) (Turetsky et al., 2014). The first two mechanisms increase FCH₄ while the
634 latter decrease FCH₄. Similar to other studies (Chu et al., 2014; Morin et al., 2014; Rinne et al.,
635 2018), GPP was found to be among the top predictors of FCH₄ at the seasonal scale across
636 multiple sites, although it always followed temperature in relative importance (Fig. 3, Fig. S3).
637 The relationship between GPP and FCH₄ observed in this study supports earlier studies
638 suggesting that the relationship between GPP and FCH₄ is dominated by either the addition of
639 root exudates to the rhizosphere, particularly for deeper rooted plants, or the result of increased
640 CH₄ transport through aerenchymatous vegetation (Bellisario et al., 1999; Hargreaves et al.,
641 2001; Hatala et al., 2012a; Chu et al., 2014)

642 At the seasonal scale, FCH₄ lagged both LE (17 ± 18 days) and GPP ($\sim 13 \pm 23$ days)
643 considerably. These lags reflect the fact that GPP and LE peaked before FCH₄, similar to the
644 findings of Delwiche et al. (in review) and Mitra et al. (2020). At the seasonal scale, this lag
645 suggests a delay between labile organic carbon inputs from plants (either in the form of exudates
646 or fresh detritus) and FCH₄ (Megonigal et al., 2004). Alternatively, this delay could be caused
647 by confounding variables such as temperature (Rinne et al., 2018), again highlighting the

648 importance of considering direct drivers of CH₄ production, oxidation and transport (e.g.,
649 substrate availability, microbial composition, redox) rather than proxies (e.g., GPP) for these
650 controls as we were limited to in this study.

651 As observed in other studies, plant activity was linked to FCH₄ at the diel scale (Table 3,
652 Fig. 3, Fig. 8). While studies generally agree that plant activity controls diel variations in wetland
653 FCH₄, it is challenging to identify whether the direct mechanism is the strength of internal gas
654 transport, stomatal conductance, or stimulation of CH₄ production through a supply of
655 photosynthate as root exudates (Van der Nat & Middelburg, 2000; Hatala et al., 2012a; Morin et
656 al., 2014; Koebisch et al., 2015). Our observation that LE and VPD were generally the strongest
657 synchronous diel predictors of FCH₄ suggests that internal gas transport rather than stomatal
658 conductance (as represented by synchronous coupling between FCH₄ and GPP, NEE or SW_IN)
659 generally controls FCH₄ at the diel scale (Table 1) (Sturtevant et al., 2016; Villa et al., 2020). If
660 we consider maximum IR at the diel scale, lags with LE and VPD were small, again supporting
661 the role of VPD-pressurized ventilation mechanism as an important mechanism driving CH₄
662 exchange in these sites with aerenchymatous vegetation (Table 1, Table 2). The strong co-
663 variance of FCH₄ with LE and VPD also suggests that the physical processes that control
664 evaporation and boundary layer mixing exert very similar controls on CH₄ volatilization (Table
665 1). At four sites, maximum IR was between GPP or NEP and FCH₄, suggesting that recent
666 photosynthates may also control FCH₄ at the diel scale (Table 1), with a lag on the order of 1 to
667 4 hours (Fig. 8). These lags are comparable to other studies which found that GPP caused a
668 diurnal pattern in CH₄ emissions (Hatala et al., 2012a; Knox et al., 2016, Mitra et al. 2020).
669 However, in some cases where GPP was identified as a dominant predictor of FCH₄ at the diel

670 scale, GPP seemed to modulate the amplitude of the diel pattern rather than the shape of the diel
671 pattern in FCH₄ (Fig. S11).

672 *4.6. Limitations and next steps*

673 Though separating the time scales of variation was useful for isolating and identifying
674 dominant predictors of FCH₄, one limitation of these approaches is that they do not explicitly
675 account for dependencies and interactions among drivers (Sturtevant et al., 2016). For example,
676 temperature may be a confounding effect when interpreting the importance of LE and GPP at the
677 seasonal scale since temperature influences both of these variables. Similarly, RF variable
678 importance rankings can be susceptible to shuffling when highly correlated predictors are
679 present, though this was not observed in this study. While in this study we assume that a stronger
680 variable importance metric provides evidence that a given predictor is more important, future
681 work could explicitly consider partial or interactive effects among drivers. For instance, future
682 studies could test approaches such as conditional or partial mutual information (Frenzel &
683 Pompe, 2007; Sharma & Mehrotra, 2014; Zhao et al., 2016), conditional variable importance for
684 RF (Strobl et al., 2008), or commonality analysis and structural equation modeling (Koebsch,
685 Sonntag, et al., 2020) to characterize interactions and interdependencies among multiple
686 predictors.

687 Additionally, future research could focus on addressing causation in a similar nonlinear,
688 multiresolution framework. While the methods selected here were used due to their widespread
689 application and intuitive statistical interpretation, other methods are better suited for assessing
690 causation (Runge et al. 2019). For instance, Granger causality has been used for assigning
691 causation in environmental time series (Molini et al., 2010; Detto et al., 2012; Hatala et al.,
692 2012a). Transfer entropy, which quantifies information flow rather than simply overlap, is a

693 nonparametric information theory metric that implies causation (Schreiber, 2000). Here, we
694 focused on mutual information over transfer entropy due to its lower data requirements (Ruddell
695 & Kumar, 2009) and greater ease of interpretation (Sturtevant et al., 2016). However, future
696 work could focus on more explicitly addressing causation.

697 While 42 freshwater wetland sites are currently included in the FLUXNET-CH₄ dataset
698 (Delwiche et al., in review), the lack of ancillary measurements (most notably WTD) precluded
699 the inclusion of many sites from our analysis. Furthermore, the dataset contains far fewer sites in
700 the tropics relative to higher latitude regions (Delwiche et al., in review). As such, our analysis is
701 limited to a subset of 23 sites, predominantly located in temperate and boreal latitudes (Fig. 1).
702 The inclusion of a handful of subtropical and tropical sites in this study highlights the differences
703 in the dominant predictors of FCH₄ at the seasonal scale between low latitude, seasonal wetlands
704 and higher latitude sites (i.e., the relative importance of WTD vs. temperature). Moving forward,
705 we encourage site principal investigators to measure and report the full suite of variables listed in
706 Table 1 and to expand the number of low latitude sites so that future studies can include a larger
707 number of sites with greater spatial coverage in the tropics. This expansion can improve the
708 spatial representativeness of sites in future analyses ensuring that our understanding of wetland
709 FCH₄ does not remain biased towards temperate and high latitude regions, particularly in North
710 America and Europe (Fig. 1). It can also increase the statistical power of future studies.

711 Finally, while coupling wavelet decomposition and the statistical analyses presented here
712 provides a valuable post hoc tool for inferring controls on FCH₄ and can generally explain much
713 of the variability in FCH₄ across scales, they are empirical approaches focused on net FCH₄, and
714 therefore do not explicitly allow for direct assessment of the drivers of CH₄ production,
715 oxidation, and transport (Table 1). As mentioned above, future work could focus on better

716 integrating eddy covariance FCH₄ measurements across sites with critical but often missing
717 drivers of FCH₄. For instance, this includes direct measurements of redox potential and oxygen
718 content, substrate availability, and detailed information on soil microbial communities driving
719 CH₄ production and consumption (Kwon et al., 2017; Nemitz et al., 2018). Furthermore, this
720 could be done in a spatially explicit manner to better understand site-level heterogeneity, which
721 is something that was not directly addressed in this study due to the integrative nature of eddy
722 covariance measurements (although we did explore site-level heterogeneity to some extent by
723 including wind direction, but these variables did not come up as dominant variables in the
724 analyses). Future research should also focus on pairing eddy covariance observations with stable
725 isotope analyses of CH₄, and incubation, chamber, and leaf level measurements to provide
726 improved understanding of the direct mechanisms of CH₄ production, transport and oxidation
727 (Chanton et al., 1997; Marushchak et al., 2016; Villa et al., 2020). In particular, with respect to
728 CH₄ transport and controls on FCH₄ at the diel scale, given that the majority of the sites
729 measured FCH₄ using an open-path sensor, it is also possible that density corrections may have
730 influenced diel patterns in CH₄ exchange, and in turn the evaluation of biophysical predictors of
731 FCH₄ and associated lags (Chamberlain et al., 2017). As such, coupling eddy covariance
732 measurements with leaf chamber measurements or isotope analyses is especially useful for better
733 identifying controls on diel scale FCH₄.

734 Nonetheless, by combining multiple statistical methods in a wavelet-based multi-
735 resolution framework, this study contributes to an improved understanding of the predictors of
736 FCH₄ across a wide range of non-tidal, freshwater wetlands, which can help inform empirical
737 and process-based models of FCH₄ (Oikawa et al., 2017). As such, while our analysis does not
738 provide an explicit predictive model, it does provide the timing and scale-dependent information

739 that can help guide modeling efforts toward better representing scale-dependent, asynchronous
740 and nonlinear processes inherent in FCH₄ (Sturtevant et al., 2016), thereby helping better
741 constrain wetland CH₄ emissions.

742 **5. Acknowledgements**

743
744 We acknowledge primary support from the Gordon and Betty Moore Foundation (Grant
745 GBMF5439, “Advancing Understanding of the Global Methane Cycle”; Stanford University)
746 and from the John Wesley Powell Center for Analysis and Synthesis of the U.S. Geological
747 Survey (“Wetland FLUXNET Synthesis for Methane” working group). Benjamin R. K. Runkle
748 was supported by the National Science Foundation (NSF) Award 1752083. Masahito Ueyama
749 was supported by ArCS II (JPMXD1420318865) and JSPS KAKENHI (20K21849). William J.
750 Riley and Qing Zhu were supported by the U.S. Department of Energy (DOE) BER-RGCM-
751 RUBISCO project (DEAC02-05CH11231). Jessica Turner acknowledges support from NSF
752 GRFP (DGE-1747503) and NTL LTER (DEB-1440297). Minseok Kang was supported by the
753 National Research Foundation of Korea (NRF-2018 R1C1B6002917). Rodrigo Vargas
754 acknowledges support from NSF (grant #1652594). Dennis Baldocchi acknowledges the
755 California Department of Water Resources for a funding contract from the California
756 Department of Fish and Wildlife and the U.S. Department of Agriculture (NIFA grant #2011-
757 67003-30371). Oliver Sonnentag acknowledges funding by the Canada Research Chairs, Canada
758 Foundation for Innovation Leaders Opportunity Fund, and Natural Sciences and Engineering
759 Research Council Discovery Grant Programs for work at CA-SCB. Benjamin Poulter
760 acknowledges support from the NASA Carbon Cycle and Ecosystems Program. Gil Bohrer
761 acknowledges funding by DOE (DE-SC0021067) and the Ohio Department of Natural Resources
762 (Subaward N18B 315-11). Pavel Alekseychik acknowledges support from the CLIMOSS project

763 funded by the Academy of Finland (grant #296116), and the SOMPA project funded by the
764 Strategic Research Council at the Academy of Finland (grant #312912). Tuula Aalto and
765 Annalea Lohila acknowledge the support from the Academy of Finland project UPFORMET
766 (grant #307331). Eeva-Stiina Tuittila acknowledges support from the Academy of Finland
767 (grants #287039 and #330840). Mats Nilsson and Matthias Peichl acknowledge support from the
768 Swedish national research infrastructure ICOS and SITES and from the Swedish Research
769 Council, Swedish Research Council for Environment, Agricultural Sciences and Spatial Planning
770 and the Kempe Foundation. Pia Gottschalk acknowledges support from the German Federal
771 Ministry of Food and Agriculture (BMEL) within the ERA-NET FACCE ERA-GAS, with
772 FACCE ERA-GAS received funding from the European Union's Horizon 2020 Research and
773 Innovation Programme (grant #696356). The FI-Lom, FI-Sii, and SE-Deg sites are part of the
774 ICOS European Research Infrastructure. We acknowledge the following AmeriFlux sites for
775 their data records: US-Uaf, US-Los, US-Myb, US-OWC, US-Tw1, US-Tw4, US-WPT, US-
776 MAC. In addition, funding for AmeriFlux data resources and core site data was provided by the
777 DOE's Office of Science.

778

779

780

781 **References**

- 782 Abdi, H., & Williams, L. J. (2010). Principal component analysis. *Wiley Interdisciplinary*
783 *Reviews: Computational Statistics*, 2(4), 433–459. <https://doi.org/10.1002/wics.101>.
- 784 Angle, J. C., Morin, T. H., Solden, L. M., Narrowe, A. B., Smith, G. J., Borton, M. A., Rey-
785 Sanchez, C., Daly, R. A., Mirfenderesgi, G., Hoyt, D. W., Riley, W. J., Miller, C. S., Bohrer,
786 G., & Wrighton, K. C. (2017). Methanogenesis in oxygenated soils is a substantial fraction
787 of wetland methane emissions. *Nature Communications*, 8(1567).
788 <https://doi.org/10.1038/s41467-017-01753-4>.
- 789 Aurela, M., Lohila, A. Tuovinen, J.-P., Hatakka, J., Rainne, J., Mäkelä, T., and Lauria, T.
790 (2020). FLUXNET-CH4 FI-Lom Lompolojankka. Finland.
791 <https://doi:10.18140/FLX/1669638>.
- 792 Baldocchi, D. (2014). Measuring fluxes of trace gases and energy between ecosystems and the
793 atmosphere - the state and future of the eddy covariance method. *Global Change Biology*,
794 20(12), 3600–3609. <https://doi.org/10.1111/gcb.12649>.
- 795 Bansal, S., Tangen, B., & Finocchiaro, R. (2018). Diurnal patterns of methane flux from a
796 seasonal wetland: mechanisms and methodology. *Wetlands*, 38(5), 933–943.
797 <https://doi.org/10.1007/s13157-018-1042-5>.
- 798 Bansal, S., Johnson, O. F., Meier, J., & Zhu, X. (2020). Vegetation affects timing and location of
799 wetland methane emissions. *Journal of Geophysical Research: Biogeosciences*, 125,
800 e2020JG005777. <https://doi.org/10.1029/2020JG005777>.
- 801 Barber, T. R., Burke, R. A., Jr., & Sackett, W. M. (1988). Diffusive flux of methane from warm
802 wetlands. *Global Biogeochemical Cycles*, 2(4), 411–425.
803 <https://doi.org/10.1029/GB002i004p00411>.

- 804 Bellisario, L. M., Bubier, J. L., Moore, T. R., & Chanton, J. P. (1999). Controls on CH₄
805 emissions from a northern peatland. *Global Biogeochemical Cycles*, *13*(1), 81–91.
806 <https://doi.org/10.1029/1998GB900021>.
- 807 Bohrer, G., Kerns, J., Morin, T.H., Rey-Sanchez, A.C., Villa, J., and Ju, Y. (2020). FLUXNET-
808 CH₄ US-OWC Old Woman Creek. United States. <https://doi:10.18140/FLX/1669690>.
- 809 Breiman, L. (2001). Random Forests. *Machine Learning*, *45*(1), 5–32.
810 <https://doi.org/10.1023/A:1010933404324>.
- 811 Bridgham, S. D., Cadillo-Quiroz, H., Keller, J. K., & Zhuang, Q. (2013). Methane emissions
812 from wetlands: biogeochemical, microbial, and modeling perspectives from local to global
813 scales. *Global Change Biology*, *19*(5), 1325–1346. <https://doi.org/10.1111/gcb.12131>.
- 814 Bubier, J. L., Moore, T. R., Bellisario, L., Comer, N. T., & Crill, P. M. (1995). Ecological
815 controls on methane emissions from a northern peatland complex in the zone of
816 discontinuous permafrost, Manitoba, Canada. *Global Biogeochemical Cycles*, *9*(4), 455–
817 470. <https://doi.org/10.1029/95gb02379>.
- 818 Campbell, D., and Goodrich, J. (2020). FLUXNET-CH₄ NZ-Kop Kopuatai. New Zealand.
819 <https://doi:10.18140/FLX/1669652>.
- 820 Casper, P., Maberly, S. C., Hall, G. H., & Finlay, B. J. (2000). Fluxes of methane and carbon
821 dioxide from a small productive lake to the atmosphere. *Biogeochemistry*, *49*(1), 1–19.
822 <https://doi.org/10.1023/A:1006269900174>.
- 823 Chamberlain, S. D., Verfaillie, J., Eichelmann, E., Hemes, K. S., & Baldocchi, D. D. (2017).
824 Evaluation of density corrections to methane fluxes measured by open-path eddy covariance
825 over contrasting landscapes. *Boundary-Layer Meteorology*, *165*(2), 197–210.
826 <https://doi.org/10.1007/s10546-017-0275-9>.

- 827 Chang, K., Riley, W. J., Brodie, E. L., McCalley, C. K., Crill, P. M., & Grant, R. F. (2019).
828 Methane production pathway regulated proximally by substrate availability and distally by
829 temperature in a high-latitude mire complex. *Journal of Geophysical Research:*
830 *Biogeosciences*, *124*(10), 3057–3074. <https://doi.org/10.1029/2019JG005355>.
- 831 Chang, K. Y., W. J. Riley, S. H. Knox, R. B. Jackson, G. McNicol, B. Poulter, M. Aurela, D.
832 Baldocchi, S. Bansal, G. Bohrer, D. I. Campbell, A. Cescatti, H. Chu, K. B. Delwiche, A.
833 Desai, E. Euskirchen, T. Friborg, M. Goeckede, G. Holm, M. Kang, T. Keenan, K. W.
834 Krauss, A. Lohila, I. Mammarella, A. Miyata, & Others (2021). Global wetland methane
835 emissions have hysteretic responses to seasonal temperature. *Nature Communications*, *12*,
836 2266, <https://doi.org/10.1038/s41467-021-22452-1>.
- 837 Chanton, J. P., Martens, C. S., & Kelley, C. A. (1989). Gas transport from methane-saturated,
838 tidal freshwater and wetland sediments. *Limnology and Oceanography*, *34*(5), 807–819.
839 <https://doi.org/10.4319/lo.1989.34.5.0807>.
- 840 Chanton, J. P., Whiting, G. J., Blair, N. E., Lindau, C. W., & Bollich, P. K. (1997). Methane
841 emission from rice: Stable isotopes, diurnal variations, and CO₂ exchange. *Global*
842 *Biogeochemical Cycles*, *11*(1), 15–27. <https://doi.org/10.1029/96GB03761>.
- 843 Chen, J., and Housen Chu. (2020). FLUXNET-CH4 US-WPT Winous Point North Marsh.
844 United States. doi:10.18140/FLX/1669702.
- 845 Chen, W., Zhang, F., Wang, B., Wang, J., Tian, D., Han, G., Wen, X., Yu, G., & Niu, S. (2019).
846 Diel and seasonal dynamics of ecosystem-scale methane flux and their determinants in an
847 alpine meadow. *Journal of Geophysical Research: Biogeosciences*, *124*(6), 1731–1745.
848 <https://doi.org/10.1029/2019jg005011>.

- 849 Chen, X., Schäfer, K. V. R., & Slater, L. (2017). Methane emission through ebullition from an
850 estuarine mudflat: 2. Field observations and modeling of occurrence probability. *Water*
851 *Resources Research*, 53(8), 6439–6453. <https://doi.org/10.1002/2016wr019720>.
- 852 Christensen, T. R., Ekberg, A., Ström, L., Mastepanov, M., Panikov, N., Öquist, M., Svensson,
853 B. H., Nykänen, H., Martikainen, P. J., & Oskarsson, H. (2003). Factors controlling large
854 scale variations in methane emissions from wetlands. *Geophysical Research Letters*, 30(7),
855 261. <https://doi.org/10.1029/2002GL016848>.
- 856 Chu, H., Chen, J., Gottgens, J. F., Ouyang, Z., John, R., Czajkowski, K., & Becker, R. (2014).
857 Net ecosystem methane and carbon dioxide exchanges in a Lake Erie coastal marsh and a
858 nearby cropland. *Journal of Geophysical Research: Biogeosciences*, 119(5), 722–740.
859 <https://doi.org/10.1002/2013JG002520>.
- 860 Cornish, C. R., D. B. Percival, and C. S. Bretherton (2003). The WMTSA Wavelet Toolkit for
861 data analysis in the geosciences. *Eos Trans. AGU*, 84(46), Fall Meet. Suppl., Abstract
862 NG11A-0173.
- 863 Delwiche, K. B., Knox, S. H., Malhotra, A., Fluet-Chouinard, E., McNicol, G., Feron, S.,
864 Ouyang, Z., Papale, D., Trotta, C., Canfora, E., Chea, Y.-W., Christianson, D., Alberto, M.
865 C. R., Alekseychik, P., Aurela, M. & Others. (In Review). FLUXNET-CH4: A global,
866 multi-ecosystem dataset and analysis of methane seasonality from freshwater wetlands.
867 *Earth System Science Data*.
- 868 Desai, A. R., Xu, K., Tian, H., Weishampel, P., Thom, J., Baumann, D., Andrews, A. E., Cook,
869 B. D., King, J. Y., & Kolka, R. (2015). Landscape-level terrestrial methane flux observed
870 from a very tall tower. *Agricultural and Forest Meteorology*, 201, 61–75.
871 <https://doi.org/10.1016/j.agrformet.2014.10.017>.

- 872 Desai, A. R., and Thom, J. (2020). FLUXNET-CH4 US-Los Lost Creek. United States.
873 <https://doi.org/10.18140/FLX/1669682>.
- 874 Detto, M., Molini, A., Katul, G., Stoy, P., Palmroth, S., & Baldocchi, D. (2012). Causality and
875 persistence in ecological systems: a nonparametric spectral granger causality approach. *The*
876 *American Naturalist*, *179*(4), 524–535. <https://doi.org/10.1086/664628>.
- 877 Eichelmann, E., Knox, S., Rey-Sanchez, A.C, Valach, A., Sturtevant, C., Szutu, D., Verfaillie, J.,
878 and Baldocchi, D. (2020). FLUXNET-CH4 US-Tw4 Twitchell East End Wetland. United
879 States. <https://doi.org/10.18140/FLX/1669698>.
- 880 Engle, D., & Melack, J. M. (2000). Methane emissions from an Amazon floodplain lake:
881 Enhanced release during episodic mixing and during falling water. *Biogeochemistry*, *51*(1),
882 71–90. <https://doi.org/10.1023/A:1006389124823>.
- 883 Etminan, M., Myhre, G., Highwood, E. J., & Shine, K. P. (2016). Radiative forcing of carbon
884 dioxide, methane, and nitrous oxide: A significant revision of the methane radiative forcing.
885 *Geophysical Research Letters*, *43*(24), 12,614–12,623.
886 <https://doi.org/10.1002/2016gl071930>.
- 887 Fechner-Levy, E. J., & Hemond, H. F. (1996). Trapped methane volume and potential effects on
888 methane ebullition in a northern peatland. *Limnology and Oceanography*, *41*(7), 1375–1383.
889 <https://doi.org/10.4319/lo.1996.41.7.1375>.
- 890 Fraser, A. M., & Swinney, H. L. (1986). Independent coordinates for strange attractors from
891 mutual information. *Physical Review A: General Physics*, *33*(2), 1134–1140.
892 <https://doi.org/10.1103/physreva.33.1134>.

- 893 Frenzel, S., & Pompe, B. (2007). Partial mutual information for coupling analysis of multivariate
894 time series. *Physical Review Letters*, *99*(20), 204101.
895 <https://doi.org/10.1103/PhysRevLett.99.204101>.
- 896 Genuer, R., Poggi, J.-M., & Tuleau-Malot, C. (2010). Variable selection using random forests.
897 *Pattern Recognition Letters*, *31*(14), 2225–2236.
898 <https://doi.org/10.1016/j.patrec.2010.03.014>.
- 899 Goodrich, J. P., Campbell, D. I., Roulet, N. T., Clearwater, M. J., & Schipper, L. A. (2015).
900 Overriding control of methane flux temporal variability by water table dynamics in a
901 Southern Hemisphere, raised bog. *Journal of Geophysical Research: Biogeosciences*,
902 *120*(5), 819–831. <https://doi.org/10.1002/2014JG002844>.
- 903 Gregory R. Warnes, Ben Bolker, Lodewijk Bonebakker, Robert Gentleman, Wolfgang Huber
904 Andy Liaw, Thomas Lumley, Martin Maechler, Arni Magnusson, Steffen Moeller, Marc
905 Schwartz and Bill Venables. (2019). gplots: Various R programming tools for plotting data.
906 <https://cran.r-project.org/web/packages/gplots/index.html>.
- 907 Hargreaves, K. J., Fowler, D., Pitcairn, C. E. R., & Aurela, M. (2001). Annual methane emission
908 from Finnish mires estimated from eddy covariance campaign measurements. *Theoretical
909 and Applied Climatology*, *70*(1), 203–213. <https://doi.org/10.1007/s007040170015>.
- 910 Hatala, J. A., Detto, M., & Baldocchi, D. D. (2012a). Gross ecosystem photosynthesis causes a
911 diurnal pattern in methane emission from rice. *Geophysical Research Letters*, *39*(6).
912 <https://doi.org/10.1029/2012GL051303>.
- 913 Hatala, J. A., Detto, M., Sonnentag, O., Deverel, S. J., Verfaillie, J., & Baldocchi, D. D. (2012b).
914 Greenhouse gas (CO₂, CH₄, H₂O) fluxes from drained and flooded agricultural peatlands in

- 915 the Sacramento-San Joaquin Delta. *Agriculture, Ecosystems & Environment*, *150*, 1–18.
916 <https://doi.org/10.1016/j.agee.2012.01.009>.
- 917 Hollinger, D. Y., & Richardson, A. D. (2005). Uncertainty in eddy covariance measurements and
918 its application to physiological models. *Tree Physiology*, *25*(7), 873–885.
919 <https://doi.org/10.1093/treephys/25.7.873>.
- 920 Iwata, H. (2020a). FLUXNET-CH4 JP-Mse Mase rice paddy field. Japan.
921 <https://doi:10.18140/FLX/1669647>.
- 922 Iwata, H., Ueyama M., and Harazono, Y. (2020b). FLUXNET-CH4 US-Uaf University of
923 Alaska, Fairbanks. United States. Web. <https://doi:10.18140/FLX/1669701>.
- 924 Jackson, R. B., Saunio, M., Bousquet, P., Canadell, J. G., Poulter, B., Stavert, A. R.,
925 Bergamaschi, P., Niwa, Y., Segers, A., & Tsuruta, A. (2020). Increasing anthropogenic
926 methane emissions arise equally from agricultural and fossil fuel sources. *Environmental*
927 *Research Letters*, *15*, 071002. <https://doi.org/10.1088/1748-9326/ab9ed2>.
- 928 Jammet, M., Dengel, S., Kettner, E., Parmentier, F.-J. W., Wik, M., Crill, P., & Friborg, T.
929 (2017). Year-round CH₄ and CO₂ flux dynamics in two contrasting freshwater ecosystems of
930 the subarctic. *Biogeosciences*, *14*(22), 5189–5216. <https://doi.org/10.5194/bg-14-5189-2017>.
- 931 Kim, D.-G., Vargas, R., Bond-Lamberty, B., & Turetsky, M. R. (2012). Effects of soil rewetting
932 and thawing on soil gas fluxes: a review of current literature and suggestions for future
933 research. *Biogeosciences*, *9*(7), 2459–2483. <https://doi.org/10.5194/bg-9-2459-2012>.
- 934 Kim, Y., Johnson, M. S., Knox, S. H., Andrew Black, T., Dalmagro, H. J., Kang, M., Kim, J., &
935 Baldocchi, D. (2020). Gap-filling approaches for eddy covariance methane fluxes: A
936 comparison of three machine learning algorithms and a traditional method with principal

- 937 component analysis. *Global Change Biology*, 26(3), 1499–1518.
- 938 <https://doi.org/10.1111/gcb.14845>.
- 939 Knoblauch, C., Spott, O., Evgrafova, S., Kutzbach, L., & Pfeiffer, E. (2015). Regulation of
940 methane production, oxidation, and emission by vascular plants and bryophytes in ponds of
941 the northeast Siberian polygonal tundra. *Journal of Geophysical Research: Biogeosciences*,
942 120(12), 2525–2541. <https://doi.org/10.1002/2015JG003053>.
- 943 Knox, S. H., Matthes, J. H., Sturtevant, C., Oikawa, P. Y., Verfaillie, J., & Baldocchi, D. (2016).
944 Biophysical controls on interannual variability in ecosystem-scale CO₂ and CH₄ exchange in
945 a California rice paddy. *Journal of Geophysical Research: Biogeosciences*, 121(3), 978–
946 1001. <https://doi.org/10.1002/2015JG003247>.
- 947 Knox, S. H., Jackson, R. B., Poulter, B., McNicol, G., Fluet-Chouinard, E., Zhang, Z., Hugelius,
948 G., Bousquet, P., Canadell, J. G., Saunois, M., Papale, D., Chu, H., Keenan, T. F.,
949 Baldocchi, D., Torn, M. S., Mammarella, I., Trotta, C., Aurela, M., Bohrer, G., & Others.
950 (2019). FLUXNET-CH₄ synthesis activity: objectives, observations, and future directions.
951 *Bulletin of the American Meteorological Society*, 100(12), 2607–2632.
952 <https://doi.org/10.1175/BAMS-D-18-0268.1>.
- 953 Knox, Sara, Matthes, J. H., Verfaillie, J., and Baldocchi, D. (2020). FLUXNET-CH₄ US-Twt
954 Twitchell Island. United States, (2020). Web. <https://doi:10.18140/FLX/1669700>.
- 955 Koebisch, F., Jurasinski, G., Koch, M., Hofmann, J., & Glatzel, S. (2015). Controls for multi-
956 scale temporal variation in ecosystem methane exchange during the growing season of a
957 permanently inundated fen. *Agricultural and Forest Meteorology*, 204, 94–105.
958 <https://doi.org/10.1016/j.agrformet.2015.02.002>.

- 959 Koebisch, F., Gottschalk, P., Beyer, F., Wille, C., Jurasinski, G., & Sachs, T. (2020a). The impact
960 of occasional drought periods on vegetation spread and greenhouse gas exchange in
961 rewetted fens. *Philosophical Transactions of the Royal Society of London, Series B,*
962 *Biological Sciences*, 375(1810), 20190685. <https://doi.org/10.1098/rstb.2019.0685>.
- 963 Koebisch, F., and Jurasinski, G. (2020b). FLUXNET-CH4 DE-Hte Huetelmoor. Germany.
964 <https://doi:10.18140/FLX/1669634>.
- 965 Koebisch, F., Sonnentag, O., Järveoja, J., Peltoniemi, M., Alekseychik, P., Aurela, M., Arslan, A.
966 N., Dinsmore, K., Gianelle, D., Helfter, C., Jackowicz-Korczynski, M., Korrensalo, A.,
967 Leith, F., Linkosalmi, M., Lohila, A., Lund, M., Maddison, M., Mammarella, I., Mander, Ü.,
968 & Others. (2020c). Refining the role of phenology in regulating gross ecosystem
969 productivity across European peatlands. *Global Change Biology*, 26(2), 876–887.
970 <https://doi.org/10.1111/gcb.14905>.
- 971 Kwon, M. J., Beulig, F., Ilie, I., Wildner, M., Küsel, K., Merbold, L., Mahecha, M. D., Zimov,
972 N., Zimov, S. A., Heimann, M., Schuur, E. A. G., Kostka, J. E., Kolle, O., Hilke, I., &
973 Göckede, M. (2017). Plants, microorganisms, and soil temperatures contribute to a decrease
974 in methane fluxes on a drained Arctic floodplain. *Global Change Biology*, 23(6), 2396–
975 2412. <https://doi.org/10.1111/gcb.13558>.
- 976 Laanbroek, H. J. (2010). Methane emission from natural wetlands: interplay between emergent
977 macrophytes and soil microbial processes. A mini-review. *Annals of Botany*, 105(1), 141–
978 153. <https://doi.org/10.1093/aob/mcp201>.
- 979 Lai, D. Y. F. (2009). Methane dynamics in northern peatlands: A review. *Pedosphere*, 19(4),
980 409–421. [https://doi.org/10.1016/s1002-0160\(09\)00003-4](https://doi.org/10.1016/s1002-0160(09)00003-4).

- 981 Li, H., Dai, S., Ouyang, Z., Xie, X., Guo, H., Gu, C., Xiao, X., Ge, Z., Peng, C., & Zhao, B.
982 (2018). Multi-scale temporal variation of methane flux and its controls in a subtropical tidal
983 salt marsh in eastern China. *Biogeochemistry*, *137*(1), 163–179.
984 <https://doi.org/10.1007/s10533-017-0413-y>.
- 985 Linkhorst, A., Hiller, C., DelSontro, T., M. Azevedo, G., Barros, N., Mendonça, R., & Sobek, S.
986 (2020). Comparing methane ebullition variability across space and time in a Brazilian
987 reservoir. *Limnology and Oceanography*, *65*(7), 1623–1634.
988 <https://doi.org/10.1002/lno.11410>.
- 989 Malhotra, A., & Roulet, N. T. (2015). Environmental correlates of peatland carbon fluxes in a
990 thawing landscape: do transitional thaw stages matter? *Biogeosciences*, *12*(10), 3119–3130.
991 <https://doi.org/10.5194/bg-12-3119-2015>.
- 992 Marushchak, M. E., Friberg, T., Biasi, C., Herbst, M., Johansson, T., Kiepe, I., Liimatainen, M.,
993 Lind, S. E., Martikainen, P. J., Virtanen, T., Soegaard, H., & Shurpali, N. J. (2016). Methane
994 dynamics in the subarctic tundra: combining stable isotope analyses, plot- and ecosystem-
995 scale flux measurements. *Biogeosciences*, *13*(2), 597–608. [https://doi.org/10.5194/bg-13-](https://doi.org/10.5194/bg-13-597-2016)
996 [597-2016](https://doi.org/10.5194/bg-13-597-2016).
- 997 Matthes, J.H., Sturtevant, C., Oikawa, P., Chamberlain, S.D., Szutu, D., Ortiz A. A., Verfaillie,
998 J., and Baldocchi, D. (2020). FLUXNET-CH4 US-Myb Mayberry Wetland. United States.
999 <https://doi:10.18140/FLX/1669685>.
- 1000 Mattson, M. D., & Likens, G. E. (1990). Air pressure and methane fluxes. *Nature*, *347*(6295),
1001 718–719. <https://doi.org/10.1038/347718b0>.
- 1002 McNicol, G., Sturtevant, C. S., Knox, S. H., Dronova, I., Baldocchi, D. D., & Silver, W. L.
1003 (2017). Effects of seasonality, transport pathway, and spatial structure on greenhouse gas

- 1004 fluxes in a restored wetland. *Global Change Biology*, 23(7), 2768–2782.
- 1005 <https://doi.org/10.1111/gcb.13580>.
- 1006 Megonigal, J. P., Hines, M. E., & Visscher, P. T. (2004). Anaerobic metabolism: linkages to
1007 trace gases and aerobic processes. In Schlesinger, W., Holland, H. and Turekian, K. (Eds.),
1008 Treatise on Geochemistry (Volume 8, pp. 317-424). Elsevier.
- 1009 Mitra, B., Minick, K., Miao, G., Domec, J.-C., Prajapati, P., McNulty, S. G., Sun, G., King, J. S.,
1010 & Noormets, A. (2020). Spectral evidence for substrate availability rather than
1011 environmental control of methane emissions from a coastal forested wetland. *Agricultural
1012 and Forest Meteorology*, 291, 108062. <https://doi.org/10.1016/j.agrformet.2020.108062>.
- 1013 Molini, A., Katul, G. G., & Porporato, A. (2010). Causality across rainfall time scales revealed
1014 by continuous wavelet transforms. *Journal of Geophysical Research*, 115(D14), 579.
1015 <https://doi.org/10.1029/2009JD013016>.
- 1016 Moore, T. R., & Knowles, R. (1989). The influence of water table levels on methane and carbon
1017 dioxide emissions from peatland soils. *Canadian Journal of Soil Science*, 69(1), 33–38.
1018 <https://doi.org/10.4141/cjss89-004>.
- 1019 Moore, T. R., & Dalva, M. (1993). The influence of temperature and water table position on
1020 carbon dioxide and methane emissions from laboratory columns of peatland soils. *Journal of
1021 Soil Science*, 44(4), 651–664. <https://doi.org/10.1111/j.1365-2389.1993.tb02330.x>.
- 1022 Morin, T. H., Bohrer, G., Frasson, R. P. d. M., Naor-Azreli, L., Mesi, S., Stefanik, K. C., &
1023 Schäfer, K. V. R. (2014). Environmental drivers of methane fluxes from an urban temperate
1024 wetland park. *Journal of Geophysical Research: Biogeosciences*, 119(11), 2188–2208.
1025 <https://doi.org/10.1002/2014JG002750>.

- 1026 Morin, T. H. (2019). Advances in the eddy covariance approach to CH₄ monitoring over two and
1027 a half decades. *Journal of Geophysical Research: Biogeosciences*, *124*(3), 453–460.
1028 <https://doi.org/10.1029/2018JG004796>.
- 1029 Nadeau, D. F., Rousseau, A. N., Coursolle, C., Margolis, H. A., & Parlange, M. B. (2013).
1030 Summer methane fluxes from a boreal bog in northern Quebec, Canada, using eddy
1031 covariance measurements. *Atmospheric Environment*, *81*, 464–474.
1032 <https://doi.org/10.1016/j.atmosenv.2013.09.044>.
- 1033 Nemitz, E., Mammarella, I., Ibrom, A., Aurela, M., Burba, G. G., Dengel, S., Gielen, B., Grelle,
1034 A., Heinesch, B., Herbst, M., & Others. (2018). Standardisation of eddy-covariance flux
1035 measurements of methane and nitrous oxide. *International Agrophysics*, *32*(4), 517–549.
1036 <https://doi:10.1515/intag-2017-0042>.
- 1037 Nilsson, M. B., and Peichl, M. (2020). FLUXNET-CH₄ SE-Deg Degero. Sweden.
1038 <https://doi:10.18140/FLX/1669659>.
- 1039 Oikawa, P. Y., Jenerette, G. D., Knox, S. H., Sturtevant, C., Verfaillie, J., Dronova, I.,
1040 Poindexter, C. M., Eichelmann, E., & Baldocchi, D. D. (2017). Evaluation of a hierarchy of
1041 models reveals importance of substrate limitation for predicting carbon dioxide and methane
1042 exchange in restored wetlands. *Journal of Geophysical Research: Biogeosciences*, *122*(1),
1043 145–167. <https://doi.org/10.1002/2016JG003438>.
- 1044 Olefeldt, D., Turetsky, M. R., Crill, P. M., & David McGuire, A. (2013). Environmental and
1045 physical controls on northern terrestrial methane emissions across permafrost zones. *Global*
1046 *Change Biology*, *19*(2), 589–603. <https://doi.org/10.1111/gcb.12071>.
- 1047 Olson, D. M., Dinerstein, E., Wikramanayake, E. D., Burgess, N. D., Powell, G. V. N.,
1048 Underwood, E. C., D'amico, J. A., Itoua, I., Strand, H. E., Morrison, J. C., Loucks, C. J.,

- 1049 Allnutt, T. F., Ricketts, T. H., Kura, Y., Lamoreux, J. F., Wettengel, W. W., Hedao, P., &
1050 Kassem, K. R. (2001). Terrestrial ecoregions of the world: A new map of life on Earth.
1051 *BioScience*, *51*(11), 933. [https://doi.org/10.1641/0006-3568\(2001\)051\[0933:teotwa\]2.0.co;2](https://doi.org/10.1641/0006-3568(2001)051[0933:teotwa]2.0.co;2).
- 1052 Peltola, O., Vesala, T., Gao, Y., Rätty, O., Alekseychik, P., Aurela, M., Chojnicki, B., Desai, A.
1053 R., Dolman, A. J., Euskirchen, E. S., Friborg, T., Göckede, M., Helbig, M., Humphreys, E.,
1054 Jackson, R. B., Jocher, G., Joos, F., Klatt, J., Knox, S. H., & Others. (2019). Monthly
1055 gridded data product of northern wetland methane emissions based on upscaling eddy
1056 covariance observations. *Earth System Science Data*, *11*(3), 1263–1289.
1057 <https://doi.org/10.5194/essd-11-1263-2019>.
- 1058 Perryman, C. R., McCalley, C. K., Malhotra, A., Florencia Fahnestock, M., Kashi, N. N., Bryce,
1059 J. G., Giesler, R., & Varner, R. K. (2020). Thaw transitions and redox conditions drive
1060 methane oxidation in a permafrost peatland. *Journal of Geophysical Research:*
1061 *Biogeosciences*, *125*(3). <https://doi.org/10.1029/2019jg005526>.
- 1062 Pugh, C. A., Reed, D. E., Desai, A. R., & Sulman, B. N. (2018). Wetland flux controls: how does
1063 interacting water table levels and temperature influence carbon dioxide and methane fluxes
1064 in northern Wisconsin? *Biogeochemistry*, *137*(1), 15–25. [https://doi.org/10.1007/s10533-](https://doi.org/10.1007/s10533-017-0414-x)
1065 [017-0414-x](https://doi.org/10.1007/s10533-017-0414-x).
- 1066 Pypker, T. G., Moore, P. A., Hribljan, J. A., & Chimner, R. (2013). Shifting environmental
1067 controls on CH₄ fluxes in a sub-boreal peatland. *Biogeosciences*, *10*, 7971-7981.
1068 <https://doi.org/10.5194/bg-10-7971-2013>.
- 1069 R Core Team. (2019). R: A language and environment for statistical computing. R Foundation
1070 for Statistical Computing. <https://www.R-project.org/>

- 1071 Rinne, J., Tuittila, E.-S., Peltola, O., Li, X., Raivonen, M., Alekseychik, P., Haapanala, S.,
1072 Pihlatie, M., Aurela, M., Mammarella, I., & Vesala, T. (2018). Temporal variation of
1073 ecosystem scale methane emission from a boreal fen in relation to temperature, water table
1074 position, and carbon dioxide fluxes. *Global Biogeochemical Cycles*, 32(7), 1087–1106.
1075 <https://doi.org/10.1029/2017gb005747>.
- 1076 Ruddell, B. L., Sturtevant, C., Kang, M., & Yu, R. (2008). ProcessNetwork Software (Version
1077 1.5) [Computer software]. Retrieved from
1078 https://github.com/ProcessNetwork/ProcessNetwork_Software.
- 1079 Ruddell, B. L., & Kumar, P. (2009). Ecohydrologic process networks: 1. Identification. *Water*
1080 *Resources Research*, 45(3). <https://doi.org/10.1029/2008WR007279>.
- 1081 Runge J., Bathiany, S., Bollt, E., Camps-Valls, G., Coumou, D., Deyle, E., Glymour, C.,
1082 Kretschmer, M., Mahecha, M., Muñoz-Mari, J., van Nes, E., Peters, J., Quax, R., Reichstein,
1083 M., Scheffer, M., Schölkopf, B., Spirtes, P., Sugihara, G., Sun, J., Zhang, K. & Zscheischler,
1084 J. (2019). Inferring causation from time series in Earth system sciences. *Nature:*
1085 *Communications*, 10:2553. <https://doi.org/10.1038/s41467-019-10105-3>.
- 1086 Runkle, B. R. K., Suvočarev, K., Reba, M. L., Reavis, C. W., Smith, S. F., Chiu, Y.-L., & Fong,
1087 B. (2019). Methane Emission Reductions from the Alternate Wetting and Drying of Rice
1088 Fields Detected Using the Eddy Covariance Method. *Environmental Science & Technology*,
1089 53(2), 671–681. <https://doi.org/10.1021/acs.est.8b05535>.
- 1090 Ryu, Youngryel, Kang, M., and Kim, J. (2020). FLUXNET-CH4 KR-CRK Cheorwon Rice
1091 paddy. Korea, Republic of. doi:10.18140/FLX/1669649.

- 1092 Sachs, T., Wille, C., Boike, J., & Kutzbach, L. (2008). Environmental controls on ecosystem-
1093 scale CH₄ emission from polygonal tundra in the Lena River Delta, Siberia. *Journal of*
1094 *Geophysical Research: Biogeosciences*, *113*(G3). <https://doi.org/10.1029/2007JG000505>.
- 1095 Sachs, T., Wille, C., Larmanou, E., and Franz, D. (2020). FLUXNET-CH₄ DE-Zrk Zarnekow.
1096 Germany. <https://doi:10.18140/FLX/1669636>.
- 1097 Sakabe, A., Itoh, M., Hirano, T., and Kusin, K. (2020). FLUXNET-CH₄ ID-Pag Palangkaraya
1098 undrained forest. Indonesia. <https://doi:10.18140/FLX/1669643>.
- 1099 Saunio, M., Stavert, A. R., Poulter, B., Bousquet, P., Canadell, J. G., Jackson, R. B., Raymond,
1100 P. A., Dlugokencky, E. J., Houweling, S., Patra, P. K., Ciais, P., Arora, V. K., Bastviken, D.,
1101 Bergamaschi, P., Blake, D. R., Brailsford, G., Bruhwiler, L., Carlson, K. M., Carrol, M.,
1102 Castaldi, S., Chandra, N., Crevoisier, C., Crill, P. M., Covey, K., Curry, C. L., Etiope, &
1103 Others. (2020). The global methane budget 2000--2017. *Earth System Science Data*, *12*(3),
1104 1561–1623. <https://doi.org/10.5194/essd-12-1561-2020>.
- 1105 Savi, F., Di Bene, C., Canfora, L., Mondini, C., & Fares, S. (2016). Environmental and
1106 biological controls on CH₄ exchange over an evergreen Mediterranean forest. *Agricultural*
1107 *and Forest Meteorology*, *226-227*, 67–79. <https://doi.org/10.1016/j.agrformet.2016.05.014>
- 1108 Schäfer, K. V. R., Tripathee, R., Artigas, F., Morin, T. H., & Bohrer, G. (2014). Carbon dioxide
1109 fluxes of an urban tidal marsh in the Hudson-Raritan estuary. *Journal of Geophysical*
1110 *Research: Biogeosciences*, *119*(11), 2065–2081. <https://doi.org/10.1002/2014jg002703>.
- 1111 Schaller, C., Kittler, F., Foken, T., & Göckede, M. (2019). Characterisation of short-term
1112 extreme methane fluxes related to non-turbulent mixing above an Arctic permafrost
1113 ecosystem. *Atmospheric Chemistry and Physics*, *19*(6), 4041–4059. [https://doi:10.5194/acp-](https://doi:10.5194/acp-19-4041-2019)
1114 [19-4041-2019](https://doi:10.5194/acp-19-4041-2019).

- 1115 Schreiber, T. (2000). Measuring information transfer. *Physical Review Letters*, *85*(2), 461–464.
1116 <https://doi.org/10.1103/PhysRevLett.85.461>.
- 1117 Seyfferth, A. L., Bothfeld, F., Vargas, R., Stuckey, J. W., Wang, J., Kearns, K., Michael, H. A.,
1118 Guimond, J., Yu, X., & Sparks, D. L. (2020). Spatial and temporal heterogeneity of
1119 geochemical controls on carbon cycling in a tidal salt marsh. *Geochimica et Cosmochimica*
1120 *Acta*, *282*, 1–18. <https://doi.org/10.1016/j.gca.2020.05.013>.
- 1121 Sharma, A., & Mehrotra, R. (2014). An information theoretic alternative to model a natural
1122 system using observational information alone. *Water Resources Research*, *50*(1), 650–660.
1123 <https://doi.org/10.1002/2013wr013845>.
- 1124 Song, C., Sun, L., Huang, Y., Wang, Y., & Wan, Z. (2011). Carbon exchange in a freshwater
1125 marsh in the Sanjiang Plain, northeastern China. *Agricultural and Forest Meteorology*,
1126 *151*(8), 1131–1138. <https://doi.org/10.1016/j.agrformet.2011.04.001>.
- 1127 Sonnentag, O., and Helbig, M. (2020). FLUXNET-CH4 CA-SCB Scotty Creek Bog. Canada.
1128 <https://doi:10.18140/FLX/1669613>.
- 1129 Sparks, J.P. (2020). FLUXNET-CH4 US-MAC MacArthur Agro-Ecology. United States.
1130 <https://doi:10.18140/FLX/1669683>.
- 1131 Strachan, I. B., Nugent, K. A., Crombie, S., & Bonneville, M.-C. (2015). Carbon dioxide and
1132 methane exchange at a cool-temperate freshwater marsh. *Environmental Research Letters*,
1133 *10*(6), 065006. <https://doi.org/10.1088/1748-9326/10/6/065006>.
- 1134 Strobl, C., Boulesteix, A.-L., Zeileis, A., & Hothorn, T. (2007). Bias in random forest variable
1135 importance measures: illustrations, sources, and a solution. *BMC Bioinformatics*, *8*, 25.
1136 <https://doi.org/10.1186/1471-2105-8-25>.

- 1137 Strobl, C., Boulesteix, A.-L., Kneib, T., Augustin, T., & Zeileis, A. (2008). Conditional variable
1138 importance for random forests. *BMC Bioinformatics*, *9*:307. doi:10.1186/1471-2105-9-307.
- 1139 Sturtevant, C., Ruddell, B. L., Knox, S. H., Verfaillie, J., Matthes, J. H., Oikawa, P. Y., &
1140 Baldocchi, D. (2016). Identifying scale-emergent, nonlinear, asynchronous processes of
1141 wetland methane exchange. *Journal of Geophysical Research: Biogeosciences*, *121*(1), 188–
1142 204. <https://doi.org/10.1002/2015JG003054>.
- 1143 Wong, G.X., Melling, L., Tang, A.C.I., Aeries, E.B., Waili, J.W., Musin, K.K., Lo, K.S., and
1144 Kiew, F. (2020). FLUXNET-CH4 MY-MLM Maludam National Park. Malaysia.
1145 <https://doi:10.18140/FLX/1669650>.
- 1146 Tittel, J., Hüls, M., & Koschorreck, M. (2019). Terrestrial vegetation drives methane production
1147 in the sediments of two German reservoirs. *Scientific Reports*, *9*(1), 15944.
1148 <https://doi.org/10.1038/s41598-019-52288-1>.
- 1149 Tokida, T. (2005). Ebullition of methane from peat with falling atmospheric pressure.
1150 *Geophysical Research Letters*, *32*(13), 3257. <https://doi.org/10.1029/2005GL022949>.
- 1151 Tokida, T., Miyazaki, T., Mizoguchi, M., Nagata, O., Takakai, F., Kagemoto, A., & Hatano, R.
1152 (2007). Falling atmospheric pressure as a trigger for methane ebullition from peatland.
1153 *Global Biogeochemical Cycles*, *21*(2). <https://doi.org/10.1029/2006GB002790>.
- 1154 Treat, C. C., Anthony Bloom, A., & Marushchak, M. E. (2018). Nongrowing season methane
1155 emissions-a significant component of annual emissions across northern ecosystems. *Global*
1156 *Change Biology*, *24*(8), 3331–3343. <https://doi.org/10.1111/gcb.14137>.
- 1157 Trifunovic, B., Vázquez-Lule, A., Capooci, M., Seyfferth, A. L., Moffat, C., & Vargas, R.
1158 (2020). Carbon dioxide and methane emissions from temperate salt marsh tidal creek.

- 1159 *Journal of Geophysical Research: Biogeosciences*, 125(8), 84.
1160 <https://doi.org/10.1029/2019JG005558>.
- 1161 Tuovinen, J.-P., Aurela, M., Hatakka, J., Räsänen, A., Virtanen, T., Mikola, J., Ivakhov, V.,
1162 Kondratyev, V., & Laurila, T. (2019). Interpreting eddy covariance data from heterogeneous
1163 Siberian tundra: land cover-specific methane fluxes and spatial representativeness.
1164 *Biogeosciences*, 16, 255-274. <https://doi.org/10.5194/bg-16-255-2019>.
- 1165 Turetsky, M. R., Kotowska, A., Bubier, J., Dise, N. B., Crill, P., Hornibrook, E. R. C.,
1166 Minkinen, K., Moore, T. R., Myers-Smith, I. H., Nykänen, H., Olefeldt, D., Rinne, J.,
1167 Saarnio, S., Shurpali, N., Tuittila, E.-S., Waddington, J. M., White, J. R., Wickland, K. P., &
1168 Wilmking, M. (2014). A synthesis of methane emissions from 71 northern, temperate, and
1169 subtropical wetlands. *Global Change Biology*, 20(7), 2183–2197.
1170 <https://doi.org/10.1111/gcb.12580>.
- 1171 Ueyama, M., Hirano, T., and Kominami, Y. (2020a). FLUXNET-CH4 JP-BBY Bibai bog. Japan.
1172 <https://doi:10.18140/FLX/1669646>.
- 1173 Ueyama, M., Yazaki, T., Hirano, T., Futakuchi, Y., & Okamura, M. (2020b). Environmental
1174 controls on methane fluxes in a cool temperate bog. *Agricultural and Forest Meteorology*,
1175 281, 107852. <https://doi.org/10.1016/j.agrformet.2019.107852>.
- 1176 Updegraff, K., Bridgham, S. D., Pastor, J., Weishampel, P., & Harth, C. (2001). Response of
1177 CO₂ and CH₄ emissions from peatlands to warming and water table manipulation.
1178 *Ecological Applications*, 11(2), 311. <https://doi.org/10.2307/3060891>.
- 1179 Valach, A., Szutu, D., Eichelmann, E., Knox, S., Verfaillie, J., and Baldocchi, D. (2020).
1180 FLUXNET-CH4 US-Tw1 Twitchell Wetland West Pond. United States.
1181 <https://doi:10.18140/FLX/1669696>.

- 1182 Van der Nat, F.-J., & Middelburg, J. J. (2000). Methane emission from tidal freshwater marshes.
1183 *Biogeochemistry*, 49(2), 103–121. <https://doi.org/10.1023/A:1006333225100>.
- 1184 Vesala, T., Tuittila, E.-S., Mammarella, I., and Alekseychik, P. (2020a). FLUXNET-CH4 FI-Si2
1185 Siikaneva-2 Bog. Finland. <https://doi:10.18140/FLX/1669639>.
- 1186 Vesala, T., Tuittila, E.-S., Mammarella, I., and Rinne, J. (2020b). FLUXNET-CH4 FI-Sii
1187 Siikaneva. Finland. <https://doi:10.18140/FLX/1669640>.
- 1188 Villa, J. A., Ju, Y., Stephen, T., Rey-Sanchez, C., Wrighton, K. C., & Bohrer, G. (2020).
1189 Plant-mediated methane transport in emergent and floating-leaved species of a temperate
1190 freshwater mineral-soil wetland. *Limnology and Oceanography*, 65(7), 1635–1650.
1191 <https://doi.org/10.1002/lno.11467>.
- 1192 Villa, J. A., Y. Ju, T. Yazbeck, S. Waldo, K. C. Wrighton, and G. Bohrer. (2021). Ebullition
1193 dominates methane fluxes from the water surface across different ecohydrological patches in
1194 a temperate freshwater marsh at the end of the growing season. *Science of the Total
1195 Environment*, 767, 144498. doi:<https://doi.org/10.1016/j.scitotenv.2020.144498>.
- 1196 Vourlitis, G., Dalmagro, H., Nogueira, J.S., Johnson M., and Arruda, P. (2020). FLUXNET-CH4
1197 BR-Npw Northern Pantanal Wetland. Brazil. <https://doi:10.18140/FLX/1669368>.
- 1198 Wen, X., Unger, V., Jurasinski, G., Koebisch, F., Horn, F., Rehder, G., Sachs, T., Zak, D.,
1199 Lischeid, G., Knorr, K.-H., Böttcher, M. E., Winkel, M., Bodelier, P. L. E., & Liebner, S.
1200 (2018). Predominance of methanogens over methanotrophs in rewetted fens characterized by
1201 high methane emissions. *Biogeosciences*, 15(21), 6519–6536. [https://doi.org/10.5194/bg-15-](https://doi.org/10.5194/bg-15-6519-2018)
1202 [6519-2018](https://doi.org/10.5194/bg-15-6519-2018).
- 1203 Wood, S. N. (2011). Fast stable restricted maximum likelihood and marginal likelihood
1204 estimation of semiparametric generalized linear models. *Journal of the Royal Statistical*

- 1205 *Society: Series B (Statistical Methodology)*, 73(1), 3–36. <https://doi.org/10.1111/j.1467->
1206 9868.2010.00749.x.
- 1207 Wright, M. N., & Ziegler, A. (2017). ranger: A fast implementation of random forests for high
1208 dimensional data in C++ and R. *Journal of Statistical Software*, 77(1), pp. 1–17.
1209 <https://doi.org/10.18637/jss.v077.i01>.
- 1210 Yang, W. H., McNicol, G., Teh, Y. A., Estera-Molina, K., Wood, T. E., & Silver, W. L. (2017).
1211 Evaluating the classical versus an emerging conceptual model of peatland methane
1212 dynamics. *Global Biogeochemical Cycles*, 31(9), 1435-1453.
1213 <https://doi.org/10.1002/2017GB005622>.
- 1214 Yvon-Durocher, G., Allen, A. P., Bastviken, D., Conrad, R., Gudasz, C., St-Pierre, A., Thanh-
1215 Duc, N., & del Giorgio, P. A. (2014). Methane fluxes show consistent temperature
1216 dependence across microbial to ecosystem scales. *Nature*, 507(7493), 488–491.
1217 <https://doi.org/10.1038/nature13164>.
- 1218 Zhao, J., Zhou, Y., Zhang, X., & Chen, L. (2016). Part mutual information for quantifying direct
1219 associations in networks. *Proceedings of the National Academy of Sciences*, 113(18), 5130–
1220 5135. <https://doi.org/10.1073/pnas.1522586113>.
- 1221 Zona, D., Gioli, B., Commane, R., Lindaas, J., Wofsy, S. C., Miller, C. E., Dinardo, S. J.,
1222 Dengel, S., Sweeney, C., Karion, A., -W. Chang, R. Y., Henderson, J. M., Murphy, P. C.,
1223 Goodrich, J. P., Moreaux, V., Liljedahl, A., Watts, J. D., Kimball, J. S., Lipson, D. A., &
1224 Oechel, W. C. (2016). Cold season emissions dominate the Arctic tundra methane budget.
1225 *Proceedings of the National Academy of Sciences*, 113(1), 40–45.
1226 <https://doi.org/10.1073/pnas.1516017113>.
- 1227

1228 **Tables**

1229 Table 1. Physical and biological predictors included in this analysis and references from studies
 1230 that have previously identified these variables as predictors of methane fluxes (FCH₄). Here we
 1231 consider variables that have a direct influence on methane (CH₄) production, consumption and/or
 1232 transport (white cells associated with each predictor), and variables that represent a proxy or are
 1233 correlated with a process that has a direct influence on FCH₄ (gray cells). We also include scales
 1234 at which we hypothesize that these predictors will be dominant.

| Predictor | Mechanism(s) & hypothesized scale | References |
|---|--|---|
| <i>Biological predictors</i> | | |
| Gross primary productivity (GPP) | <ul style="list-style-type: none"> • Oxygenation of zone around roots (direct driver of CH₄ consumption) (<i>diel to seasonal scale</i>) • Carbon substrate for methanogens (i.e., root exudates, root mortality, plant residue) (proxy for CH₄ production) (<i>diel to seasonal scale</i>) • Coupling between FCH₄ and leaf photosynthesis may indicate that FCH₄ is regulated by stomatal conductance (proxy for CH₄ transport) (<i>diel scale</i>) • CH₄ transport through aerenchymatous vegetation will lead to coupling between vegetation development (e.g., stalk diameter, Leaf area index (LAI)) and FCH₄ since seasonal development of the vegetation will increase the available aerenchyma area (proxy for CH₄ transport) (<i>seasonal scale</i>) | (Hatala et al., 2012b; Malhotra & Roulet, 2015; Knox et al., 2016; Rinne et al., 2018) |
| Ecosystem respiration (RECO) | <ul style="list-style-type: none"> • May describe similar effects to those that influence CH₄ production/consumption/flux (proxy for FCH₄) (<i>diel to seasonal scale</i>) • Breakdown of complex carbon compounds provides simple carbon substrates that fuel methanogenesis and CH₄ production (<i>diel to seasonal scale</i>) | (Villa et al., 2020) |
| Net ecosystem exchange (NEE) | <ul style="list-style-type: none"> • NEE is linked to plant activity (GPP) (direct effect and proxy for FCH₄) and respiration (RECO) (proxy for FCH₄) (<i>diel to seasonal scale</i>) | (Pypker et al., 2013) |
| <i>Biological and physical predictors</i> | | |
| Latent heat turbulent flux (LE) | <ul style="list-style-type: none"> • Evaporation of water and CH₄ volatilization from the water and plant surfaces are driven by similar physical mechanisms and tend to covary (proxy for CH₄ transport) (<i>diel to seasonal scale</i>) • LE is linked to plant activity (e.g., LAI is a strong determinant of LE) (proxy for CH₄ transport) (<i>seasonal scale</i>) • Influence of vapor pressure deficit (VPD)/humidity gradients on pressurized ventilation in aerenchymatous vegetation (proxy for CH₄ transport) (<i>diel scale</i>) • In some species, stomatal conductance of water vapor from the vegetation is correlated with CH₄ transport through plant tissue (proxy for CH₄ transport) (<i>diel scale</i>) | (Morin et al., 2014; Savi et al., 2016; Sturtevant et al., 2016; Morin, 2019; Villa et al., 2020) |

| <i>Physical predictors</i> | | |
|--------------------------------------|---|---|
| Air temperature (TA) | <ul style="list-style-type: none"> • Temperature-dependence of microbial CH₄ production and consumption (direct driver of CH₄ production and consumption) (<i>multiday to seasonal scale</i>) • Influence on diffusive transport in plants (direct driver of CH₄ transport) (<i>multiday to seasonal scale</i>) | (Pugh et al., 2018, Koebisch et al. 2015) |
| Soil temperature (TS) | <ul style="list-style-type: none"> • Temperature-dependence of microbial processes controlling CH₄ production and oxidation (direct driver of CH₄ production and consumption) (<i>multiday to seasonal scale</i>) • Influence on soil diffusion and ebullition of CH₄ (direct driver of CH₄ transport) (<i>multiday to seasonal scale</i>) | (Olefeldt et al., 2013; Turetsky et al., 2014; Goodrich et al., 2015; Zona et al., 2016) |
| Water table depth (WTD) | <ul style="list-style-type: none"> • Influence on soil redox conditions (direct driver of CH₄ production and consumption) (<i>multiday to seasonal scale</i>) • Influence on slow vs. rapid diffusion of CH₄ through water vs. soils, respectively (CH₄ transport) (<i>diel to multiday scale</i>) • Influence on the rates of ebullition (CH₄ transport) (<i>diel to multiday scale</i>) | (Olefeldt et al., 2013; Turetsky et al., 2014; Goodrich et al., 2015; Bansal et al. 2020; Villa et al 2021) |
| Incoming shortwave radiation (SW_IN) | <ul style="list-style-type: none"> • Influence on TA, TS, GPP, LE, and mixing of the water column (proxy for FCH₄) (<i>diel to seasonal scale</i>) • Influence of light on plant activity (proxy for CH₄ transport) (<i>diel and seasonal scale</i>) | (Savi et al., 2016) |
| Vapor pressure deficit (VPD) | <ul style="list-style-type: none"> • Influence on pressurized ventilation of CH₄ in aerenchymatous vegetation (direct influence on CH₄ transport) (<i>diel scale</i>) <hr style="border-top: 1px dashed black;"/> <ul style="list-style-type: none"> • Influence on GPP and LE (proxy for FCH₄) (<i>diel to seasonal scale</i>) • Covaries with near-surface CH₄ concentration in the air through boundary layer growth and depth (proxy for CH₄ transport) (<i>diel scale</i>) | (Chanton et al., 1997; Sturtevant et al., 2016; Chen et al., 2019; Morin, 2019) |
| Friction velocity (USTAR) | <ul style="list-style-type: none"> • Near surface turbulence can influence ebullition and diffusion, and increased turbulence can lead to increased aeration and transient flushing of CH₄ stored in soil (direct driver of CH₄ transport) (<i>diel to multiday scale</i>) | (Sachs et al., 2008; Nadeau et al., 2013, Koebisch et al. 2015) |
| Atmospheric pressure (PA) | <ul style="list-style-type: none"> • Atmospheric pressure (falling pressure) as a trigger for methane ebullition (direct driver of CH₄ transport) (<i>diel to multiday scale</i>) | (Tokida, 2005; Tokida et al., 2007; Sachs et al., 2008; Linkhorst et al., 2020;) |
| Wind direction (WD)* | <ul style="list-style-type: none"> • Related to site heterogeneity (indirect relationship with FCH₄) (<i>diel to seasonal scale</i>) <p>*Note that WD was separated into sine and cosine of wind direction (sinWD, cosWD) to represent WD as a continuous function.</p> | (Jammet et al., 2017; Tuovinen et al., 2019) |

1236 Table 2. Description of study sites. For vegetation cover, 0 = absent and 1 = present.

| Site ID | Country | Lat | Long | Wetland Type | Biome | Management regime | Start year | End year | Mean CH ₄ flux (nmol m ⁻² s ⁻¹) | Median CH ₄ flux (nmol m ⁻² s ⁻¹) |
|---------|-------------|---------|----------|--------------|------------------------|-------------------|------------|----------|---|---|
| CA-SCB | Canada | 61.308 | -121.298 | Bog | Boreal | Natural | 2014 | 2016 | 53.71 | 52.02 |
| FI-Si2 | Finland | 61.837 | 24.197 | Bog | Boreal | Natural | 2012 | 2016 | 46.11 | 34.40 |
| US-Uaf | USA | 64.866 | -147.856 | Bog | Boreal | Natural | 2011 | 2018 | 2.66 | 1.80 |
| JP-BBY | Japan | 43.323 | 141.811 | Bog | Temperate | Natural | 2015 | 2018 | 64.99 | 58.13 |
| NZ-Kop | New Zealand | -37.388 | 175.554 | Bog | Temperate | Natural | 2012 | 2015 | 47.03 | 43.84 |
| FI-Sii | Finland | 61.833 | 24.193 | Fen | Boreal | Natural | 2013 | 2018 | 35.40 | 19.10 |
| SE-Deg | Sweden | 64.182 | 19.557 | Fen | Boreal | Natural | 2014 | 2018 | 31.65 | 21.63 |
| US-Los | USA | 46.083 | -89.979 | Fen | Boreal | Natural | 2014 | 2018 | 18.43 | 8.63 |
| DE-Hte | Germany | 54.210 | 12.176 | Fen | Temperate | Restored | 2011 | 2018 | 166.88 | 123.77 |
| DE-Zrk | Germany | 53.876 | 12.889 | Fen | Temperate | Restored | 2016 | 2018 | 80.70 | 21.30 |
| FI-Lom | Finland | 67.997 | 24.209 | Fen | Temperate | Natural | 2006 | 2010 | 49.71 | 31.50 |
| US-Myb | USA | 38.050 | -121.765 | Marsh | Temperate | Restored | 2011 | 2018 | 154.70 | 130.42 |
| US-OWC | USA | 41.380 | -82.513 | Marsh | Temperate | Natural | 2015 | 2016 | 627.33 | 540.92 |
| US-Tw1 | USA | 38.107 | -121.647 | Marsh | Temperate | Restored | 2012 | 2018 | 170.80 | 149.84 |
| US-Tw4 | USA | 38.103 | -121.641 | Marsh | Temperate | Restored | 2014 | 2018 | 98.63 | 79.88 |
| US-WPT | USA | 41.465 | -82.996 | Marsh | Temperate | Natural | 2011 | 2013 | 127.61 | 35.90 |
| JP-Mse | Japan | 36.054 | 140.027 | Rice | Temperate | Managed | 2012 | 2012 | 59.35 | 35.00 |
| KR-CRK | Korea | 38.201 | 127.251 | Rice | Temperate | Managed | 2015 | 2018 | 98.80 | 37.10 |
| US-Twt | USA | 38.109 | -121.653 | Rice | Temperate | Managed | 2009 | 2017 | 37.71 | 14.29 |
| US-MAC | USA | 27.163 | -81.187 | Drained | Temperate | Managed | 2013 | 2016 | 52.8 | 20.2 |
| BR-Npw | Brazil | -16.498 | -56.412 | Swamp | Tropical & Subtropical | Natural | 2015 | 2016 | 63.55 | 15.42 |
| ID-Pag | Indonesia | -2.32 | 113.9 | Swamp | Tropical & Subtropical | Natural | 2016 | 2017 | -0.42 | 0.49 |
| MY-MLM | Malaysia | 1.454 | 111.150 | Swamp | Tropical & Subtropical | Natural | 2014 | 2015 | 28.94 | 17.76 |

1237

1238

1239

1240

1241 Table 2. (cont.)

| Site ID | Moss (None) | Moss (Brown) | Moss (<i>Sphagnum</i>) | Aerenchy- matous | Erica- ceous Shrub | Tree | Data DOI/location | Data DOI Reference |
|---------|----------------|-----------------|-----------------------------|---------------------|--------------------------|------|----------------------|-------------------------|
| CA-SCB | 0 | 0 | 1 | 1 | 1 | 0 | 10.18140/FLX/1669613 | Sonnentag et al., 2020 |
| FI-Si2 | 0 | 0 | 1 | 1 | 1 | 1 | 10.18140/FLX/1669639 | Vesala et al., 2020b |
| US-Uaf | 0 | 1 | 1 | 1 | 1 | 1 | 10.18140/FLX/1669701 | Iwata et al., 2020b |
| JP-BBY | 0 | 0 | 1 | 1 | 1 | 0 | 10.18140/FLX/1669646 | Ueyama et al., 2020a |
| NZ-Kop | 0 | 0 | 1 | 1 | 0 | 0 | 10.18140/FLX/1669652 | Campbell et al., 2020 |
| FI-Sii | 0 | 0 | 1 | 1 | 0 | 0 | 10.18140/FLX/1669640 | Vesala et al., 2020a |
| SE-Deg | 0 | 0 | 1 | 1 | 1 | 0 | 10.18140/FLX/1669659 | Nilsson et al., 2020 |
| US-Los | 1 | 0 | 0 | 1 | 1 | 1 | 10.18140/FLX/1669682 | Desai et al., 2020 |
| DE-Hte | 1 | 0 | 0 | 1 | 0 | 0 | 10.18140/FLX/1669634 | Koebisch et al., 2020b |
| DE-Zrk | 1 | 0 | 0 | 1 | 0 | 0 | 10.18140/FLX/1669636 | Sachs et al., 2020 |
| FI-Lom | 0 | 1 | 1 | 1 | 1 | 0 | 10.18140/FLX/1669638 | Aurela et al., 2020 |
| US-Myb | 1 | 0 | 0 | 1 | 0 | 0 | 10.18140/FLX/1669685 | Matthes et al., 2020 |
| US-OWC | 1 | 0 | 0 | 1 | 0 | 0 | 10.18140/FLX/1669690 | Bohrer et al., 2020 |
| US-Tw1 | 1 | 0 | 0 | 1 | 0 | 0 | 10.18140/FLX/1669696 | Valach et al., 2020 |
| US-Tw4 | 1 | 0 | 0 | 1 | 0 | 0 | 10.18140/FLX/1669698 | Eichelmann et al., 2020 |
| US-WPT | 1 | 0 | 0 | 1 | 0 | 0 | 10.18140/FLX/1669702 | Chen et al., 2020 |
| JP-Mse | 1 | 0 | 0 | 1 | 0 | 0 | 10.18140/FLX/1669647 | Iwata, 2020a |
| KR-CRK | 1 | 0 | 0 | 1 | 0 | 0 | 10.18140/FLX/1669649 | Ryu et al., 2020 |
| US-Twt | 1 | 0 | 0 | 1 | 0 | 0 | 10.18140/FLX/1669700 | Knox et al., 2020 |
| US-MAC | 1 | 0 | 0 | 1 | 0 | 0 | 10.18140/FLX/1669683 | Sparks 2020 |
| BR-Npw | 1 | 0 | 0 | 1 | 0 | 1 | 10.18140/FLX/1669368 | Vourlitis et al., 2020 |
| ID-Pag | 1 | 0 | 0 | 1 | 0 | 1 | 10.18140/FLX/1669643 | Sakabe et al., 2020 |
| MY-MLM | 1 | 0 | 0 | 0 | 0 | 1 | 10.18140/FLX/1669650 | Wong et al., 2020 |

1243 Table 3. Summary of top three dominant significant predictors ($p < 0.05$) of methane flux across
 1244 sites for each time scale and statistical methods of correlation, synchronous and maximum
 1245 information theory (IR), generalized additive modeling (GAM) and random forest (RF).
 1246 Variables are defined in Table 1. Note that significance was not assessed for RF based on the
 1247 method of estimating variable importance. Analyses for ‘Seasonal’, ‘Multiday’ and ‘Diel’ time
 1248 scales were on wavelet transformed data.

| Statistical Method | Seasonal | | | Multiday | | | Diel | | | Daily average | | |
|--------------------|----------|-----|----|----------|-------|----|------|-----|-------|---------------|-----|-----|
| | #1 | #2 | #3 | #1 | #2 | #3 | #1 | #2 | #3 | #1 | #2 | #3 |
| Correlation | TS | LE | TA | PA | TA | LE | LE | NEE | SW_IN | TS | TA | GPP |
| Synchronous IR | TS | TA | LE | TS | TA | PA | LE | NEE | GPP | TS | TA | GPP |
| Maximum IR | TS | TA | LE | TS | TA | LE | NEE | LE | GPP | TS | GPP | NEE |
| GAM | TS | TA | LE | TA | sinWD | TS | LE | NEE | SW_IN | TA | TS | GPP |
| RF | TS | NEE | TA | WTD | TS | TA | NEE | LE | GPP | TS | GPP | WTD |

1249

1250

1251 **Figure legends**

1252 Figure 1. Locations of non-tidal, freshwater wetland eddy covariance sites included in this
1253 analysis of methane flux, with sites colored by wetland type. More information on these sites is
1254 provided in Table 2.

1255
1256 Figure 2. Variance of methane flux (FCH₄) wavelet coefficients at each time scale of interest as
1257 a percentage of the total variance for all sites in Table 2. The color of site labels indicates
1258 wetland type as defined in Table 2, and include bogs (pink), drained (orange), fens (green),
1259 marshes (blue), rice paddies (red), and swamps (gray). Note that the time scales of variation are
1260 described in Section 2.2.1. See Table 2 for site information and Table 1 for predictor variable
1261 information.

1262
1263 Figure 3. Heatmap of normalized, maximum relative mutual information (IR) between methane
1264 flux (FCH₄) and biophysical variables within sites for the (a) seasonal scale, (b) multiday scale,
1265 (c) diel scale, and (d) daily average scale. Analyses for a-c were conducted on wavelet
1266 transformed data. Colors range from light yellow (lowest normalized IR) to dark red (highest
1267 normalized IR). Note that non-significant IR values are shaded white. Sites are colored by
1268 wetland type as defined in Table 2 and Fig. 1, which includes bogs (pink), drained (orange), fens
1269 (green), marshes (blue), rice paddies (red), and swamps (gray). See Table 2 for site information
1270 and Table 1 for predictor variable information.

1271
1272 Figure 4. Biplots showing the two largest components from the principal component analysis of
1273 the matrix of normalized, maximum IR at the (a) seasonal scale, and (b) multiday scale. In (a)
1274 sites are colored by wetland type and the size of the dots represent the ratio of the standard
1275 deviation (SD) in WTD to SD in TA at the site. Direction and importance of normalized,
1276 maximum IR is illustrated by the vectors. See Table 2 for site information and Table 1 for
1277 predictor variable information.

1278 Figure 5. Histogram of the lag (inferred from maximum IR) between methane flux (FCH₄) and
1279 (a) WTD (7 sites, median lag = 17 days and mean lag = 18.3 days), (b) TA (19 sites, median lag
1280 = 8 days and mean lag = 10.8 days), (c) TS at depth where IR at zero lag was greatest (17 sites,
1281 median lag = 5 days and mean lag = 5.4 days), (d) LE (16 sites, median lag = 17 days and mean
1282 lag = 20.2 days), and (e) GPP (10 sites, median lag = 12.5 days and mean lag = 20.7 days). Red
1283 line indicates zero lag, dashed black line represents median lag across sites, and solid black line
1284 represents mean lag across sites. Note that the variable number of sites is due to the fact that we
1285 only included sites where the driver of interest (i.e., WTD, TA or TS) was statistically significant
1286 and in the top five highest ranked predictors. See Table 2 for site information and Table 1 for
1287 predictor variable information.

1288 Figure 6. Relative mutual information (IR) as a function of lag between wavelet transformed
1289 multiday methane flux (FCH₄) and (a) PA, (c) temperature (TA or TS depending on which had
1290 the highest IR, and (e) WTD. For ease of visualization only sites where drivers were the top
1291 predictor of multiday FCH₄ are included here. Vertical lines represent zero lag ($\tau = 0$) (dotted
1292 red line), and the mean (black line) and median (dashed black line) lag of maximum IR across
1293 sites. IR across all sites and lags were significant. Wavelet detail reconstruction of FCH₄ and (b)
1294 PA (note the negative sign for ease of visualization) for JP-BBY, (d) TS for DE-Zrk, and (f)

1295 WTD for US-Tw1. Note that the mean is removed in wavelet detail reconstructions, therefore the
1296 y-axes are relative rather than absolute. Panels (b), (d), and (f) illustrate an example of the
1297 relationships observed in panels (a), (c), and (e). See Table 2 for site information and Table 1 for
1298 predictor information.

1299 Figure 7. Average diel variation in the wavelet detail reconstruction for methane flux (FCH₄)
1300 and the predictor at maximum IR, with the lead or lag (τ) at which it occurred (in hours, positive
1301 and negative values indicate FCH₄ lagging and leading predictors, respectively). Note that the
1302 mean is removed in wavelet detail reconstructions; therefore, the y-axes are relative rather than
1303 absolute. Sites are colored by wetland type as defined in Table 2, bogs (pink), drained (orange),
1304 fens (green), marshes (blue), rice paddies (red), and swamps (gray). Also note that we used net
1305 ecosystem production (NEP) (i.e., -net ecosystem exchange [NEE]) for ease of visualization.
1306 See Table 2 for site information and Table 1 for predictor variable information.

1307
1308 Figure 8. Conceptual diagram summarizing the dominant predictors of methane flux (FCH₄)
1309 across methods, including median leads and lags identified from the IR analysis, across sites and
1310 time scales. Variables are sorted by importance by the most dominant (outer ring) to least (inner
1311 ring). Directional arrows indicate significant leads (right arrow) and lags (left arrow) of
1312 corresponding predictor with the same color. Predictors are air temperature (TA), soil
1313 temperature (TS), water table depth (WTD), latent heat turbulent flux (LE), gross primary
1314 productivity (GPP), net ecosystem exchange (NEE), air pressure (PA), and vapor pressure deficit
1315 (VPD); more predictor details in Table 1.

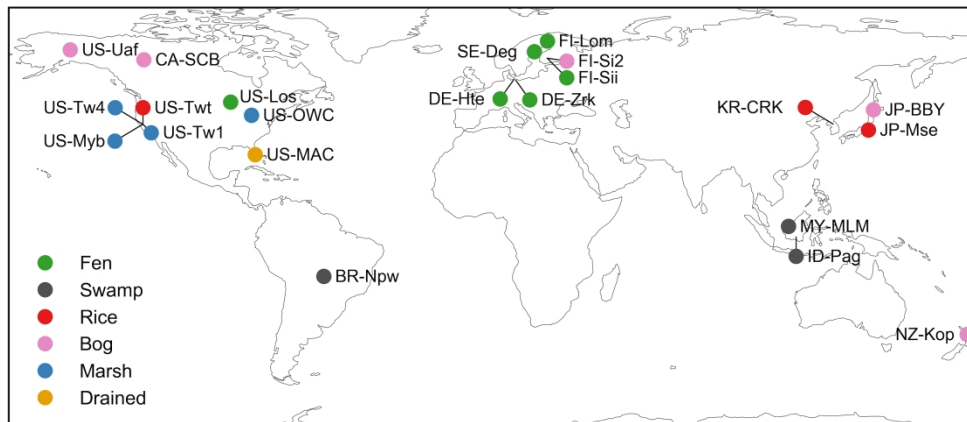


Figure 1. Locations of non-tidal, freshwater wetland eddy covariance sites included in this analysis of methane flux, with sites colored by wetland type. More information on these sites is provided in Table 2.

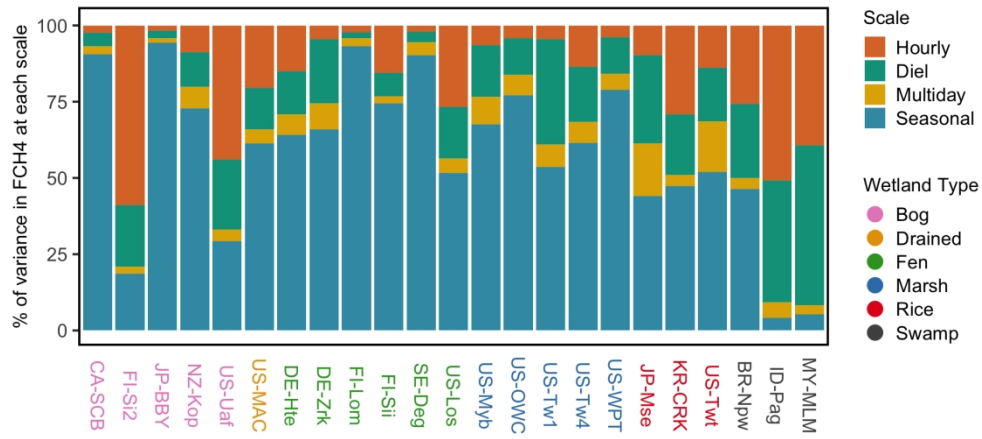


Figure 2. Variance of methane flux (FCH₄) wavelet coefficients at each time scale of interest as a percentage of the total variance for all sites in Table 2. The color of site labels indicates wetland type as defined in Table 2, and include bogs (pink), drained (orange), fens (green), marshes (blue), rice paddies (red), and swamps (gray). Note that the time scales of variation are described in Section 2.2.1. See Table 2 for site information and Table 1 for predictor variable information.

704x333mm (72 x 72 DPI)

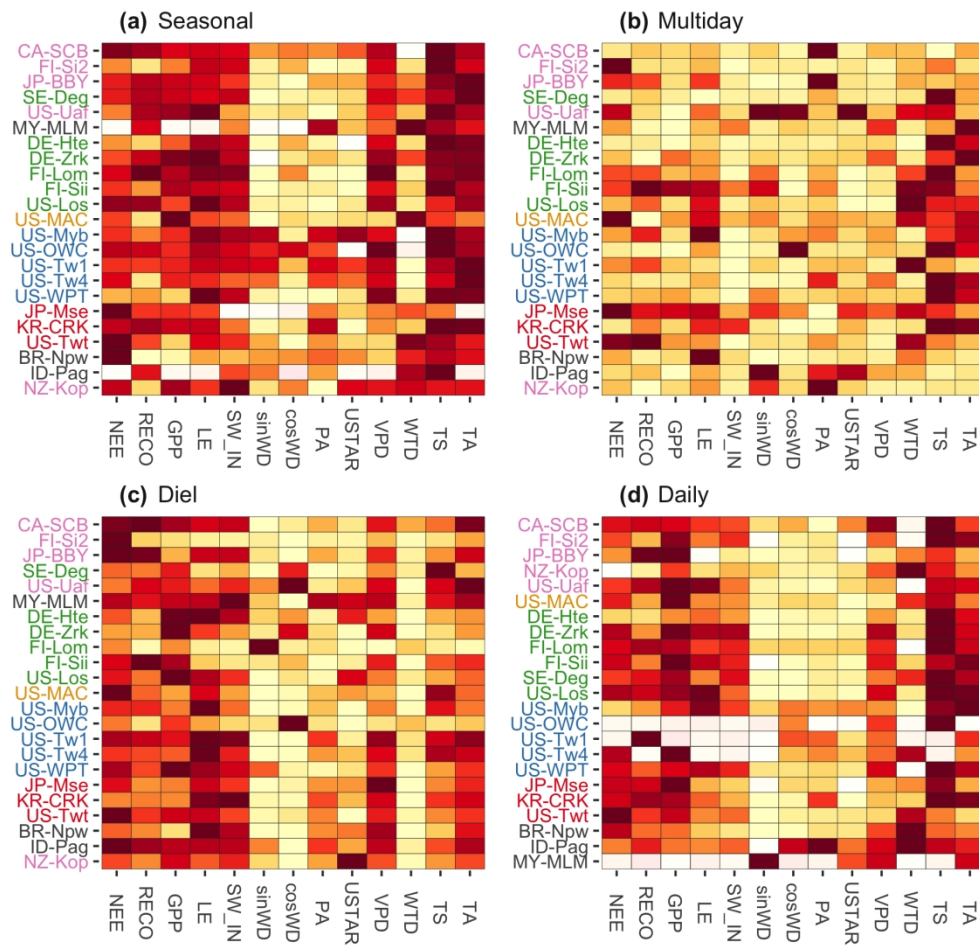


Figure 3. Heatmap of normalized, maximum relative mutual information (IR) between methane flux (FCH₄) and biophysical variables within sites for the (a) seasonal scale, (b) multiday scale, (c) diel scale, and (d) daily average scale. Analyses for a-c were conducted on wavelet transformed data. Colors range from light yellow (lowest normalized IR) to dark red (highest normalized IR). Note that non-significant IR values are shaded white. Sites are colored by wetland type as defined in Table 2 and Fig. 1, which includes bogs (pink), drained (orange), fens (green), marshes (blue), rice paddies (red), and swamps (gray). See Table 2 for site information and Table 1 for predictor variable information.

704x666mm (72 x 72 DPI)

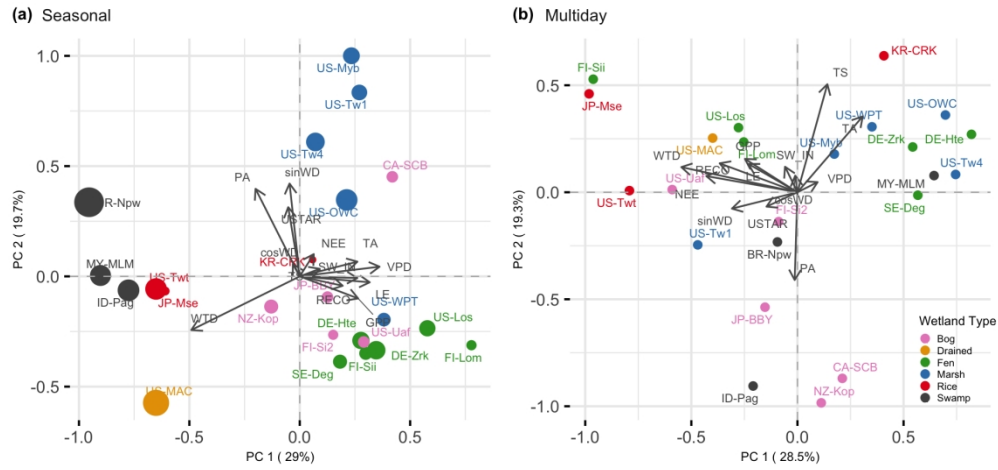


Figure 4. Biplots showing the two largest components from the principal component analysis of the matrix of normalized, maximum IR at the (a) seasonal scale, and (b) multiday scale. In (a) sites are colored by wetland type and the size of the dots represent the ratio of the standard deviation (SD) in WTD to SD in TA at the site. Direction and importance of normalized, maximum IR is illustrated by the vectors. See Table 2 for site information and Table 1 for predictor variable information.

704x333mm (72 x 72 DPI)

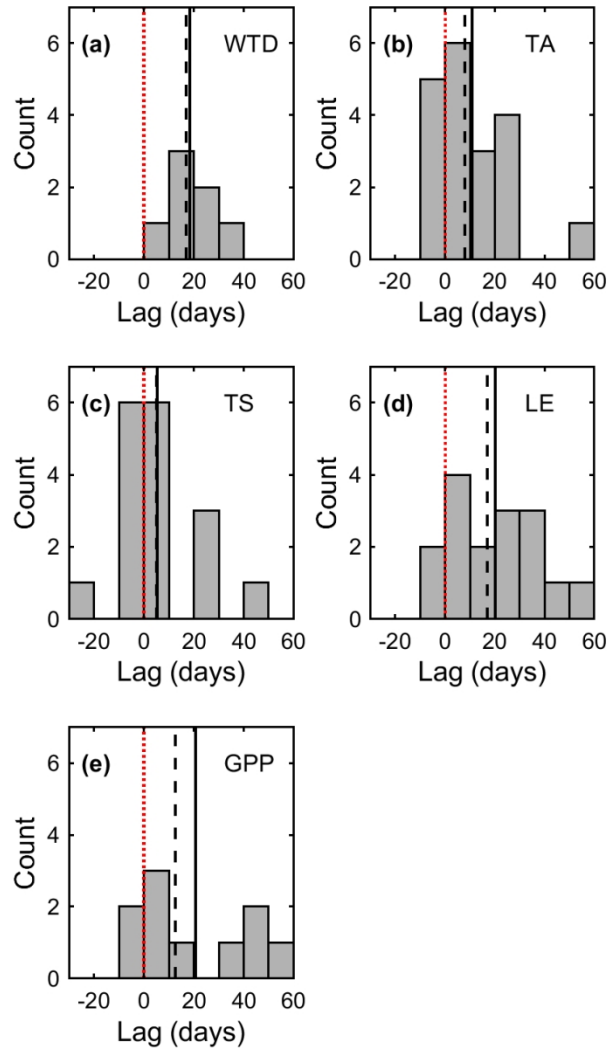


Figure 5. Histogram of the lag (inferred from maximum IR) between methane flux (FCH₄) and (a) WTD (7 sites, median lag = 17 days and mean lag = 18.3 days), (b) TA (19 sites, median lag = 8 days and mean lag = 10.8 days), (c) TS at depth where IR at zero lag was greatest (17 sites, median lag = 5 days and mean lag = 5.4 days), (d) LE (16 sites, median lag = 17 days and mean lag = 20.2 days), and (e) GPP (10 sites, median lag = 12.5 days and mean lag = 20.7 days). Red line indicates zero lag, dashed black line represents median lag across sites, and solid black line represents mean lag across sites. Note that the variable number of sites is due to the fact that we only included sites where the driver of interest (i.e., WTD, TA or TS) was statistically significant and in the top five highest ranked predictors. See Table 2 for site information and Table 1 for predictor variable information.

80x140mm (300 x 300 DPI)

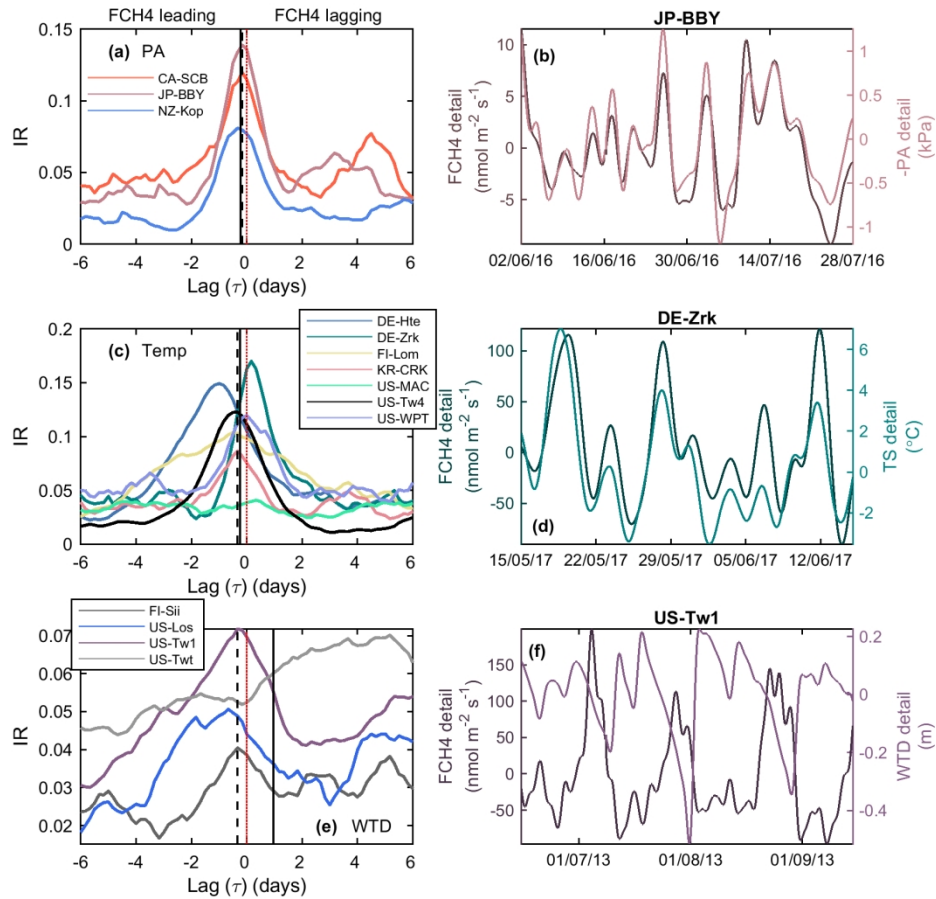


Figure 6. Relative mutual information (IR) as a function of lag between wavelet transformed multiday methane flux (FCH4) and (a) PA, (c) temperature (TA or TS depending on which had the highest IR), and (e) WTD. For ease of visualization only sites where drivers were the top predictor of multiday FCH4 are included here. Vertical lines represent zero lag ($\tau = 0$) (dotted red line), and the mean (black line) and median (dashed black line) lag of maximum IR across sites. IR across all sites and lags were significant. Wavelet detail reconstruction of FCH4 and (b) PA (note the negative sign for ease of visualization) for JP-BBY, (d) TS for DE-Zrk, and (f) WTD for US-Tw1. Note that the mean is removed in wavelet detail reconstructions, therefore the y-axes are relative rather than absolute. Panels (b), (d), and (f) illustrate an example of the relationships observed in panels (a), (c), and (e). See Table 2 for site information and Table 1 for predictor information.

160x160mm (300 x 300 DPI)

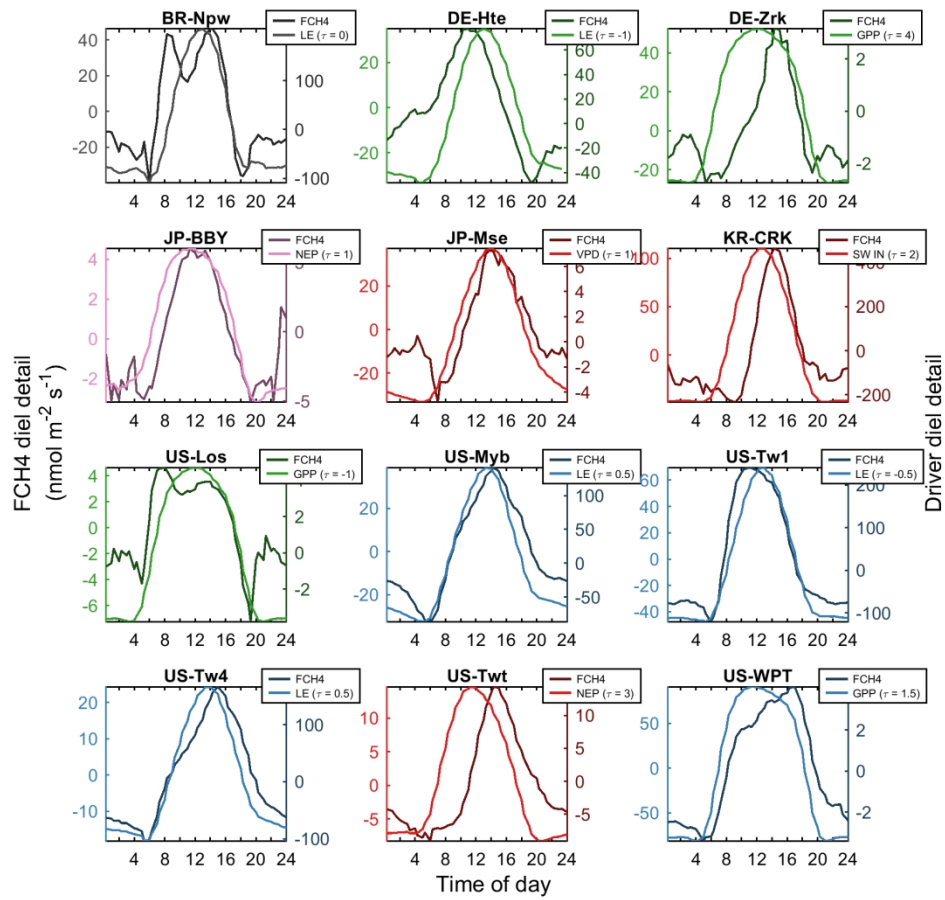


Figure 7. Average diel variation in the wavelet detail reconstruction for methane flux (FCH4) and the predictor at maximum IR, with the lead or lag (◆◆) at which it occurred (in hours, positive and negative values indicate FCH4 lagging and leading predictors, respectively). Note that the mean is removed in wavelet detail reconstructions; therefore, the y-axes are relative rather than absolute. Sites are colored by wetland type as defined in Table 2, bogs (pink), drained (orange), fens (green), marshes (blue), rice paddies (red), and swamps (gray). Also note that we used net ecosystem production (NEP) (i.e., -net ecosystem exchange [NEE]) for ease of visualization. See Table 2 for site information and Table 1 for predictor variable information.

160x160mm (300 x 300 DPI)

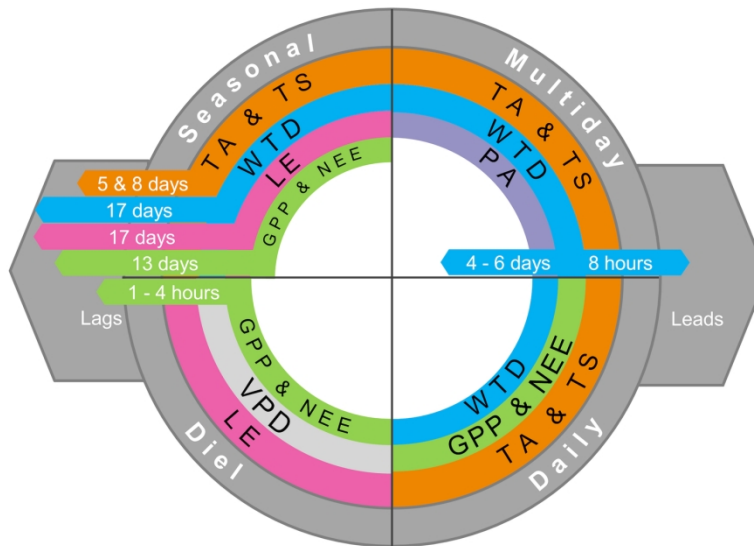


Figure 8. Conceptual diagram summarizing the dominant predictors of methane flux (FCH₄) across methods, including median leads and lags identified from the IR analysis, across sites and time scales. Variables are sorted by importance by the most dominant (outer ring) to least (inner ring). Directional arrows indicate significant leads (right arrow) and lags (left arrow) of corresponding predictor with the same color. Predictors are air temperature (TA), soil temperature (TS), water table depth (WTD), latent heat turbulent flux (LE), gross primary productivity (GPP), net ecosystem exchange (NEE), air pressure (PA), and vapor pressure deficit (VPD); more predictor details in Table 1.

168x94mm (300 x 300 DPI)